2018

SOD1A4V aggregation alters ubiquitin homeostasis in a cell model of ALS

Natalie E. Farrawell
University of Wollongong, nfarrawe@uow.edu.au

Isabella Lambert-Smith
University of Wollongong, ials563@uowmail.edu.au

Kristen Mitchell
University of Wollongong

Jessie McKenna
University of New South Wales

Luke McAlary
University of Wollongong, *University of British Columbia*, lm259@uowmail.edu.au

See next page for additional authors

Publication Details

Farrawell, N. E., Lambert-Smith, I., Mitchell, K., McKenna, J., McAlary, L., Ciryam, P., Vine, K. L., Saunders, D. N. & Yerbury, J. J. (2018). SOD1A4V aggregation alters ubiquitin homeostasis in a cell model of ALS. Journal of Cell Science, 131 (11), jcs209122-1-jcs209122-14.

SOD1A4V aggregation alters ubiquitin homeostasis in a cell model of ALS

Abstract
A hallmark of amyotrophic lateral sclerosis (ALS) pathology is the accumulation of ubiquitylated protein inclusions within motor neurons. Recent studies suggest the sequestration of ubiquitin (Ub) into inclusions reduces the availability of free Ub, which is essential for cellular function and survival. However, the dynamics of the Ub landscape in ALS have not yet been described. Here, we show that Ub homeostasis is altered in a cell model of ALS induced by expressing mutant SOD1 ($SOD1^{A4V}$). By monitoring the distribution of Ub in cells expressing $SOD1^{A4V}$, we show that Ub is present at the earliest stages of $SOD1^{A4V}$ aggregation, and that cells containing $SOD1^{A4V}$ aggregates have greater ubiquitin-proteasome system (UPS) dysfunction. Furthermore, $SOD1^{A4V}$ aggregation is associated with the redistribution of Ub and depletion of the free Ub pool. Ubiquitomics analysis indicates that expression of $SOD1^{A4V}$ is associated with a shift of Ub to a pool of supersaturated proteins, including those associated with oxidative phosphorylation and metabolism, corresponding with altered mitochondrial morphology and function. Taken together, these results suggest that misfolded SOD1 contributes to UPS dysfunction and that Ub homeostasis is an important target for monitoring pathological changes in ALS.

Disciplines
Medicine and Health Sciences

Publication Details
Farrawell, N. E., Lambert-Smith, I., Mitchell, K., McKenna, J., McAlary, L., Ciryam, P., Vine, K. L., Saunders, D. N. & Yerbury, J. J. (2018). SOD1A4V aggregation alters ubiquitin homeostasis in a cell model of ALS. Journal of Cell Science, 131 (11), jcs209122-1-jcs209122-14.

Authors
Natalie E. Farrawell, Isabella Lambert-Smith, Kristen Mitchell, Jessie McKenna, Luke McAlary, Prajwal Ciryam, Kara L. Vine, Darren N. Saunders, and Justin J. Yerbury

© 2018. Published by The Company of Biologists Ltd | Journal of Cell Science (2018) 131, jcs209122. doi:10.1242/jcs.209122

RESEARCH ARTICLE

SOD1^{A4V} aggregation alters ubiquitin homeostasis in a cell model of ALS

Natalie E. Farrawell[1,2], Isabella Lambert-Smith[1,2], Kristen Mitchell[1,2], Jessie McKenna[3], Luke McAlary[1,2,4], Prajwal Ciryam[5,6,7], Kara L. Vine[1,2], Darren N. Saunders[3] and Justin J. Yerbury[1,2,*]

ABSTRACT

A hallmark of amyotrophic lateral sclerosis (ALS) pathology is the accumulation of ubiquitylated protein inclusions within motor neurons. Recent studies suggest the sequestration of ubiquitin (Ub) into inclusions reduces the availability of free Ub, which is essential for cellular function and survival. However, the dynamics of the Ub landscape in ALS have not yet been described. Here, we show that Ub homeostasis is altered in a cell model of ALS induced by expressing mutant SOD1 (SOD1^{A4V}). By monitoring the distribution of Ub in cells expressing SOD1^{A4V}, we show that Ub is present at the earliest stages of SOD1^{A4V} aggregation, and that cells containing SOD1^{A4V} aggregates have greater ubiquitin-proteasome system (UPS) dysfunction. Furthermore, SOD1^{A4V} aggregation is associated with the redistribution of Ub and depletion of the free Ub pool. Ubiquitomics analysis indicates that expression of SOD1^{A4V} is associated with a shift of Ub to a pool of supersaturated proteins, including those associated with oxidative phosphorylation and metabolism, corresponding with altered mitochondrial morphology and function. Taken together, these results suggest that misfolded SOD1 contributes to UPS dysfunction and that Ub homeostasis is an important target for monitoring pathological changes in ALS.

This article has an associated First Person interview with the first author of the paper.

KEY WORDS: Protein aggregation, Ubiquitin, SOD1, ALS, Supersaturation, Proteostasis, Neurodegeneration, Ubiquitomics, Degron, Proteasome

INTRODUCTION

Amyotrophic lateral sclerosis (ALS, also known as motor neuron disease, MND) is a progressive neurodegenerative disease leading to paralysis of voluntary muscles due to the death of motor neurons in the brain and spinal cord. The prognosis of ALS is poor, usually leading to death within 2 to 5 years of first symptoms. A fraction of patients also develop clinical or subclinical frontotemporal dementia (FTD) (Turner et al., 2013). In most cases of ALS, the cause remains unknown (sporadic ALS; sALS). However, ∼10% of cases are inherited (familial ALS; fALS). A large proportion (20%) of fALS cases can be attributed to mutations in the gene encoding superoxide dismutase 1 (SOD1) (Chen et al., 2013). SOD1 was the first gene discovered to cause fALS and is also the most widely studied. There are now over 20 genes known to cause ALS (Chen et al., 2013), including a growing list of genes associated with dysregulation of ubiquitin (Ub) signalling. Genetic mutations in VCP, SQSTM1, UBQLN2 and OPTN have all been associated with ALS, and are all part of the protein degradation machinery of the cell. In addition, recently discovered mutations in TBK1 (Cirulli et al., 2015) and CCNF (Williams et al., 2016) add to this growing list of degradation machinery associated with ALS. The precise role of each of these genes in the homeostasis of Ub is unknown, but Ub sequestration into insoluble inclusions is common to all forms of ALS (Ciryam et al., 2017).

Abnormal accumulation of proteins into insoluble aggregates is a hallmark of many neurodegenerative diseases, including Alzheimer's disease, Parkinson's disease, Huntington's disease and ALS (Yerbury et al., 2016). In the context of ALS, there is growing evidence that a correlation exists between protein aggregate load and neuronal loss in the ALS spinal cord (Giordana et al., 2010; Brettschneider et al., 2014; Ticozzi et al., 2010; Leigh et al., 1991; Strong et al., 2005). Our previous work showed a correlation between *in vitro* aggregation propensity and rate of disease progression (McAlary et al., 2016), suggesting that protein aggregates are intimately linked with motor neuron cell death. Recent work also indicates that protein misfolding and aggregation may be responsible for disease progression through a prion-like propagation throughout the nervous system (Strong et al., 2005; Zeineddine et al., 2015; Münch et al., 2011; Sundaramoorthy et al., 2013; Grad et al., 2014). It is unlikely that misfolding alone is responsible for the disease, and post-translational modifications also seem to play an important role (McAlary et al., 2013). One crucial post-translational modification is ubiquitylation, which is necessary for protein degradation. Degradation defects that lead to inclusion formation are associated with a tendency for cells to be dysfunctional and undergo apoptosis (Atkin et al., 2014; Tsvetkov et al., 2013; Weisberg et al., 2012).

Inclusions associated with neurodegeneration consist of a variety of proteins including proteins specific to the disease [e.g. Aβ and tau in Alzheimer's disease (Chiti and Dobson, 2006)], proteins associated with cellular quality control machinery [e.g. molecular chaperones (Sherman and Goldberg, 2001; Yerbury and Kumita, 2010) and the proteasome (Huang and Figueiredo-Pereira, 2010)] and other unrelated aggregation-prone proteins (Ciryam et al., 2013, 2015). Based on analysis of human tissue, it has been shown that a large number of proteins are supersaturated in wild-type and ALS-associated mutant cells, with cellular concentrations under wild-type conditions that exceed their predicted solubility (Ciryam et al., 2013, 2015). These supersaturated proteins are associated with the biochemical pathways underpinning a variety of

[1]Illawarra Health and Medical Research Institute, Wollongong, NSW, Australia 2522. [2]Molecular Horizons and School of Chemistry & Molecular Bioscience, University of Wollongong, NSW, Australia 2522. [3]School of Medical Sciences, Faculty of Medicine, UNSW Australia 2052. [4]Department of Physics & Astronomy, University of British Columbia, Vancouver, British Columbia, Canada V6T 2B5. [5]Department of Chemistry, University of Cambridge, Cambridge CB2 1EW, UK. [6]Department of Molecular Biosciences, Rice Institute for Biomedical Research, Northwestern University, Evanston, IL 60208-3500, USA. [7]Department of Neurology, Columbia University College of Physicians & Surgeons, New York, NY 10032-3784, USA.

*Author for correspondence (jyerbury@uow.edu.au)

D.N.S., 0000-0003-0924-0513; J.J.Y., 0000-0003-2528-7039

Received 31 July 2017; Accepted 1 May 2018

Journal of Cell Science (2018) 131, jcs209122. doi:10.1242/jcs.209122

neurodegenerative diseases. Most recently, we have shown that proteins co-aggregating with SOD1, TDP-43 (also known as TARDBP) and FUS inclusions are supersaturated (Ciryam et al., 2017), consistent with a collapse of motor neuron protein homeostasis in ALS. Others have found that the proteins that co-aggregate with c9orf72 dipeptide repeats in cell models are also supersaturated (Boeynaems et al., 2017). The composition of inclusions found in ALS varies considerably depending on whether the disease is sporadic or familial, and the genetics of the familial forms.

Ub is a pervasive feature of inclusions in ALS, regardless of underlying genetic aetiology. Ub is a versatile signalling molecule responsible for controlling an array of cellular pathways including transcription, translation, vehicle transport and apoptosis (Hershko and Ciechanover, 1998). Ub labels substrate proteins via a highly ordered multi-step enzymatic cascade with specific differences in the length and topology of poly-ubiquitin chains determining a range of signalling outcomes, including proteolytic degradation via the proteasome (Ciechanover and Brundin, 2003; Pickart, 2001). Inside cells, Ub exists in a dynamic equilibrium between free Ub and Ub conjugates, and its conjugation to proteins is controlled by the opposing actions of Ub ligases and deubiquitylating enzymes (DUBs) (Dantuma et al., 2006; Groothuis et al., 2006). Recently, it has been proposed that the sequestration of Ub into insoluble aggregates may deplete the free Ub pool required by many essential cellular processes (Groothuis et al., 2006).

Although mounting genetic and functional evidence suggests an important role for the UPS in the development of ALS pathology, the distribution and availability of Ub in ALS models has not yet been described. In the work reported here, we sought to characterise the Ub landscape in a cell-based SOD1 model of ALS (Fig. S1). By following the distribution of fluorescently labelled Ub in live cells expressing mutant SOD1 ($SOD1^{A4V}$), we show that Ub homeostasis is disrupted in cells containing aggregates of $SOD1^{A4V}$. The aggregation of $SOD1^{A4V}$ leads to an accumulation of the proteasome reporter $tdTomato^{CL1}$, indicative of UPS dysfunction. This dysfunction was further supported by the redistribution of the Ub pool and decrease in free Ub levels observed in cells with $SOD1^{A4V}$ aggregates. Moreover, ubiquitome analysis confirmed that misfolded SOD1 was associated with Ub redistribution and subsequent alterations to mitochondrial morphology. This report highlights that disruption to Ub homeostasis is associated with aggregation of misfolded proteins and may play an important role in the pathogenesis of ALS.

RESULTS

$SOD1^{A4V}$ aggregates contain Ub at the earliest detectable stages of aggregation

We previously showed that all cellular SOD1 aggregates contained Ub at the time points tested (Farrawell et al., 2015). Here, we used real-time imaging using a Ub fusion protein to follow inclusion formation in a single cell from its genesis until it had taken up a large proportion of the cytoplasm. Previous work has demonstrated that GFP–Ub fusions behave identically to endogenous Ub and provide a robust fluorescent indicator of Ub distribution (Dantuma et al., 2006). We created a mCherry–Ub fusion protein that behaved in a similar manner to the GFP fusion protein (Fig. S2). Ub was observed in foci at the earliest detectable stages of $SOD1^{A4V}$ aggregation (Fig. 1A, see insert). Ub was continuously added to inclusions throughout their formation, as was $SOD1^{A4V}$ (Fig. 1A; Fig. S3). Approximately 51% of cellular ubiquitin was detected in $SOD1^{A4V}$ aggregates (Fig. 1B).

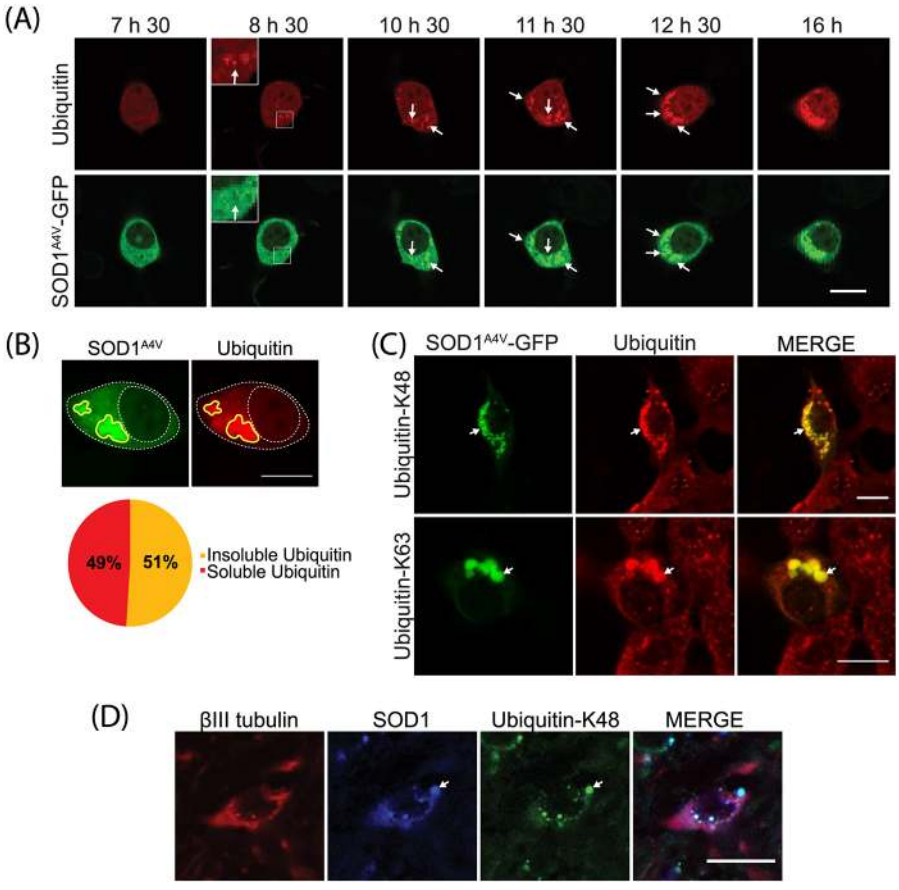

Fig. 1. $SOD1^{A4V}$ co-aggregates with Ub. (A) NSC-34 cells co-transfected with $SOD1^{A4V}$–GFP and mRFP–Ub were imaged every 15 min for 17 h. (B) Ub incorporation into $SOD1^{A4V}$ inclusions was quantified using ImageJ. (C) NSC-34 cells overexpressing $SOD1^{A4V}$–GFP were fixed, permeabilised and stained for K48-linked and K63-linked polyubiquitin chains at 48 h post transfection. (D) The spinal cord from the $SOD1^{G93A}$ mouse was fixed, permeabilised and stained for neuron-specific βIII tubulin, SOD1 and K48-linked Ub. Colocalization of SOD1 and Ub is indicated with arrows. Scale bars: 10 µm.

Journal of Cell Science (2018) 131, jcs209122. doi:10.1242/jcs.209122

To ensure that the Ub accumulation in SOD1^{A4V} inclusions was not an artefact of Ub overexpression, we next probed for endogenous Ub using antibodies. SOD1^{A4V} expression causes inclusions in ∼15% of NSC-34 cells (Fig. S4), and in those cells that contain inclusions we observed a high degree of overlap between SOD1^{A4V} aggregates and Ub when using both antibodies specific to K48 and K63 chains (Fig. 1C). We also found that SOD1^{G93A} aggregates contained Ub K48-linked chains in SOD1^{G93A} mouse spinal motor neurons (Fig. 1D).

Cells with SOD1^{A4V} aggregates have increased UPS dysfunction

We previously showed that a UPS reporter containing a CL1 degron peptide that is subject to rapid degradation accumulates to significantly higher amounts in ALS patient fibroblasts compared to controls, suggesting an overwhelmed UPS (Yang et al., 2015). Work from others suggests that SOD1 aggregates are toxic because they interfere with the quality control function of the juxtanuclear quality control compartment (JUNQ) (Weisberg et al., 2012). To examine the relationship between SOD1 aggregation and UPS dysfunction, we used transiently transfected NSC-34 cells that contained SOD1^{A4V}–GFP and tdTomato^{CL1}. We initially used flow cytometry to examine the effect of proteasome inhibition on reporter accumulation. While there was a significant difference in reporter signal between cells expressing wild-type SOD1 (SOD1^{WT}) and those expressing SOD1^{A4V}, both cell lines showed a similar dose-dependent increase in reporter signal with MG132 treatment (Fig. 2A). This suggests that, while SOD1^{A4V} expression causes significant UPS disruption, there is no specific vulnerability to proteasome inhibition of cells expressing mutant SOD1^{A4V} compared to SOD1^{WT}-expressing cells.

However, this analysis examined the entire population of SOD1^{WT}- or SOD1^{A4V}-expressing cells and previous work using a similar CL1-containing fluorescent reporter suggests that the aggregation of Huntingtin and CFTR cause UPS dysfunction (Bence et al., 2001). We hypothesised that inclusions formed by mutant SOD1 might influence UPS activity in a similar fashion, a phenomenon that may not be observed when analysing the entire population of cells, given that only 15% of NSC-34 cells expressing SOD1^{A4V} produce inclusions (Fig. S4). In order to identify cells with SOD1^{A4V} inclusions in our flow cytometry data, we tested the relationship between aggregation and total cellular fluorescence (Fig. 2B). Cells were transiently transfected with SOD1^{A4V}–GFP and imaged 48 h post transfection using confocal microscopy. The total cellular fluorescence for individual cells was plotted for both cells with and without inclusions. The fluorescence of both populations was normally distributed (Fig. 2B). The mean fluorescence of cells containing aggregates was significantly greater than that of cells without aggregates (Fig. 3C), presumably due to continued accumulation of SOD1 into inclusions. However, there was

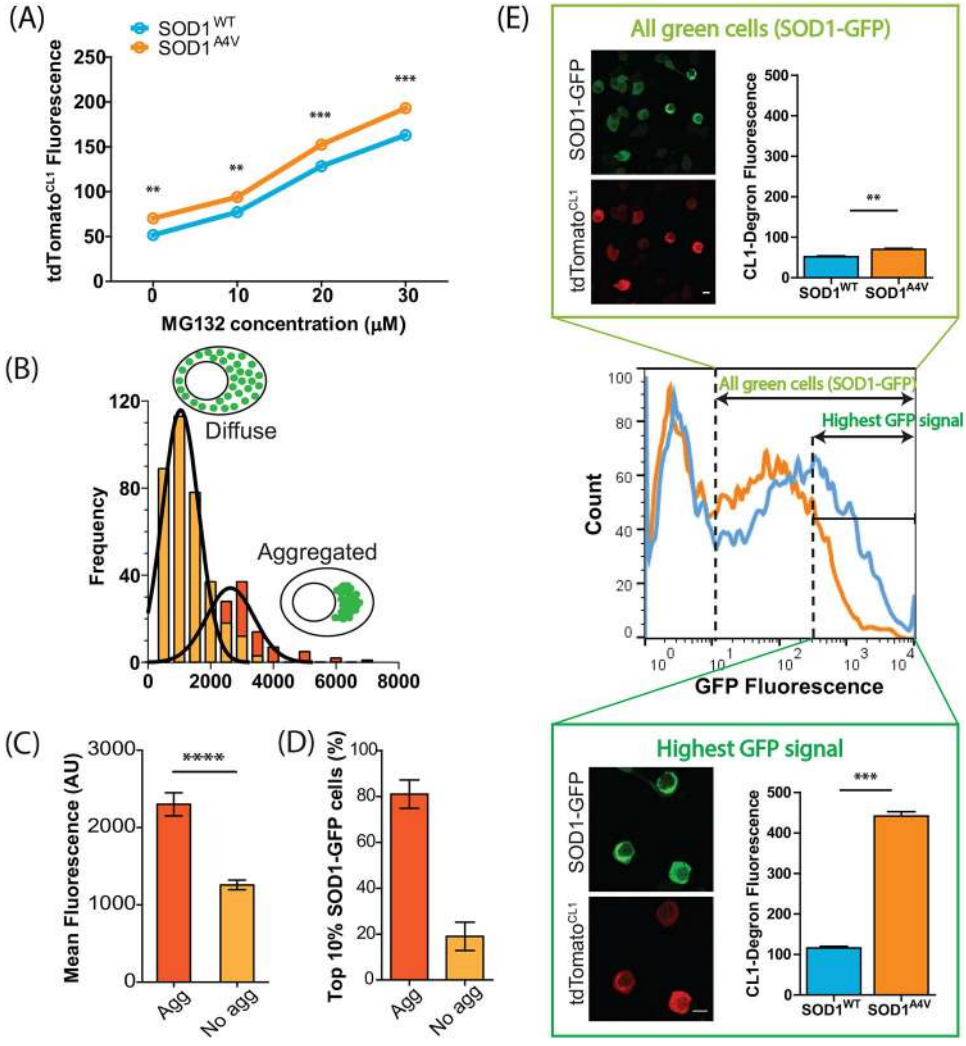

Fig. 2. Mutant SOD1^{A4V} alters UPS activity. (A) Dose-dependent response of UPS activity (tdTomato^{CL1} fluorescence) in NSC-34 cells co-transfected with SOD1^{WT}–GFP or SOD^{A4V}–GFP after overnight treatment with the indicated concentration of the proteasome inhibitor MG132. Data represent mean±s.e.m. tdTomato^{CL1} fluorescence (n=3). (B) Frequency distribution analysis of SOD1^{A4V}–GFP fluorescence was performed on cells expressing soluble (diffuse) SOD1^{A4V} and aggregated SOD1^{A4V}. (C) Cells containing SOD1^{A4V} aggregates (Agg) exhibited significantly higher fluorescence than cells that did not contain aggregates. Data shown are mean±s.e.m. (n≥100, combined from four independent experiments). (D) 80% of cells expressing the highest SOD1^{A4V}–GFP signal (top 10% of GFP-expressing cells) contained aggregates. Data shown are mean ±s.e.m. from four independent experiments where a minimum of 100 cells were counted. (E) Cells expressing the highest GFP signal (top 10% of GFP-expressing cells) typically contained aggregates and revealed greater significant differences in tdTomato^{CL1} fluorescence between cells expressing SOD1^{WT} and SOD1^{A4V}. **P<0.01; ***P<0.001; ****P<0.0001 (one-way ANOVA with a Tukey's multiple comparison post test). Scale bars: 10 µm.

Journal of Cell Science (2018) 131, jcs209122. doi:10.1242/jcs.209122

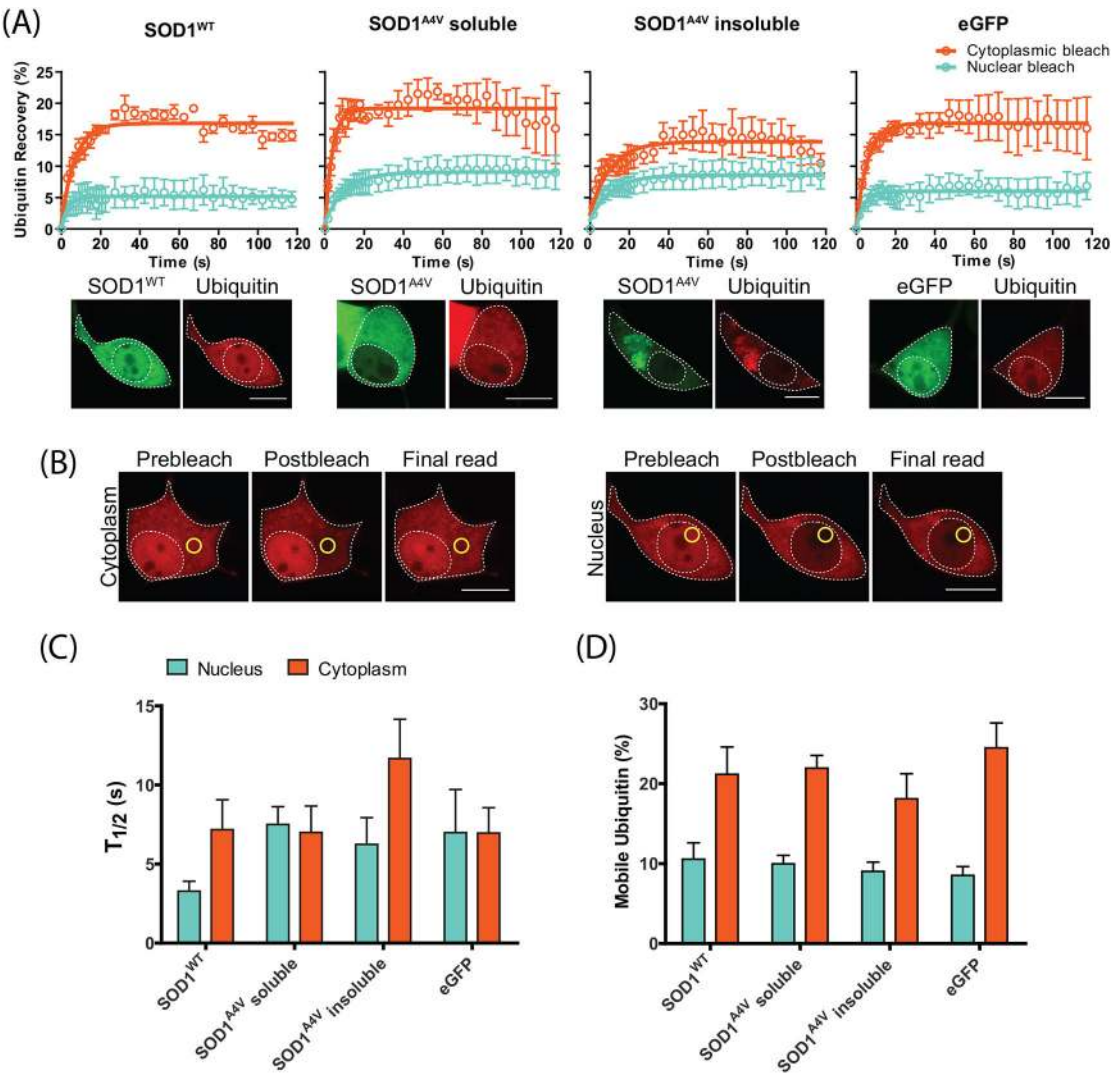

Fig. 3. Ub distribution is not significantly altered in cells containing SOD1^{A4V} aggregates. (A) NSC-34 cells co-transfected with SOD1^{WT}–GFP or SOD1^{A4V}–GFP (cells classified according to whether SOD1^{A4V} was either soluble or insoluble) and mCherry–Ub were photobleached in either the nucleus or cytoplasm, and recovery of Ub fluorescence was monitored for 120 s. Data shown are means±s.e.m. (n=3) and are representative of three independent experiments. (B) Representative confocal images of pre-bleach, post-bleach and the recovery endpoint (final read) are shown, with the ROI marked in yellow. Scale bars: 10 µm. (C) Diffusion rates ($T_{1/2}$) of mCherry–Ub measured in both the nucleus and cytoplasm of co-transfected NSC-34 cells. Data shown are means±s.e.m. (n≥6, combined from three independent experiments). (D) Quantification of the proportion of mobile Ub in the nucleus and cytoplasm of cells expressing either SOD1^{WT}, soluble SOD1^{A4V} or insoluble SOD1^{A4V}. Data shown are means±s.e.m. combined from three independent experiments (n≥7). One-way ANOVA with a Tukey's multiple comparison post-test was used to compare differences, which were not significant.

significant overlap between the two populations, so we could not entirely distinguish populations. We decided to analyse the most highly fluorescent cells (top 10%) across the entire population. In this subset of cells, ∼80% contained SOD1^{A4V} inclusions (Fig. 2D). We reasoned that analysing the top 10% fluorescent cells would sufficiently enrich for cells containing inclusions. Using flow cytometry, we observed a 4-fold increase in reporter fluorescence (P<0.001) – indicating UPS dysfunction – in the top 10% of SOD1^{A4V}–GFP-expressing cells compared to control cells (expressing SOD1^{WT}) in the same fluorescence range. That is, UPS dysfunction in SOD1^{A4V} cells is largely restricted to cells containing aggregates. By comparison, only a small increase (1.2-fold) in reporter fluorescence was observed in the entire population of SOD1^{A4V}–GFP-expressing cells compared with the entire SOD1^{WT}–GFP-expressing population (P<0.01) (Fig. 2E). This suggests that SOD1 aggregation is associated with compromised UPS function.

Ub distribution and mobility are not significantly altered in cells containing SOD1^{A4V} aggregates

Ub exists in a dynamic equilibrium in the cell, partitioning into four major pools: (1) immobile in the nucleus, (2) immobile in the cytoplasm, (3) soluble polyUb chains, and (4) a small fraction as free monomeric Ub (Dantuma et al., 2006). Mobile Ub is a combination of free monomeric Ub, free Ub chains and Ub attached to diffusible proteins (Fig. S1). Immobile Ub is primarily bound to histones in the nucleus, and bound to organelles and cytoskeleton in the cytoplasm (Fig. S1). To determine whether the observed UPS dysfunction in cells with mutant SOD1 aggregates was associated with altered Ub homeostasis, we examined the distribution of Ub into different cellular pools following expression of wild-type or mutant SOD1^{A4V} by fluorescence recovery after photobleaching (FRAP) (Fig. 3A–D). The diffusion rate back into the bleached area provides information on the mobility of the Ub species present in

Journal of Cell Science (2018) 131, jcs209122. doi:10.1242/jcs.209122

solution and the amount of immobile fluorophore in the compartment of interest (i.e. bound to membrane vesicles or cytoskeleton in the cytosol, and bound to histones in the nucleus). We selected regions of interest (ROIs) in both the nucleus and cytoplasm (Fig. 3B) in cells co-expressing mCherry–Ub and GFP, $SOD1^{WT}$–GFP or $SOD1^{A4V}$–GFP. In the case of $SOD1^{A4V}$–GFP-expressing cells, we performed the analysis on two subpopulations, cells with and without aggregates. As previously reported (Dantuma et al., 2006), we find that Ub FRAP (indicating Ub mobility) is higher in the cytoplasm than in the nucleus, likely due to a large proportion of nuclear Ub being attached to histones. Patterns of recovery appeared to be similar in all treatments, with the exception of a lower cytoplasmic recovery in the cells containing $SOD1^{A4V}$–GFP aggregates (Fig. 3A). After calculating the mean half-life ($T_{1/2}$) of recovery in each case, we find no significant differences between any of the cell populations (Fig. 3C). This suggests that, within the mobile population of Ub, the presence of $SOD1^{A4V}$–GFP aggregates does not significantly alter the kinetics of Ub diffusion. Furthermore, the amount of mobile Ub available to the cell did not appear to be altered by the presence of aggregates, as no significant differences in the mobility of Ub were observed between cells containing $SOD1^{A4V}$ aggregates and the controls (Fig. 3D).

Free monomeric Ub is lowered in cells with $SOD1^{A4V}$ aggregates

To test whether cells containing $SOD1^{A4V}$–GFP aggregates may diminish free monomeric Ub, we next examined the relative amounts of monomeric Ub in cells expressing GFP, $SOD1^{WT}$–GFP or $SOD1^{A4V}$–GFP for 48 h, by western blotting (Fig. 4A). We did not observe any significant differences using this method, likely due to the fact that this analysis represents a total measure of all cells in the culture, including non-transfected cells (Fig. S5). We therefore turned to fluorescence recovery after nucleus photobleaching (FRANP) analysis to monitor free Ub in single cells. Monomeric mCherry–Ub will diffuse through the nuclear pore (<60 kDa), while mCherry–Ub incorporated into Ub chains will not (Dantuma et al., 2006). Hence, relative free monomeric Ub can be measured by monitoring diffusion through the nuclear pore following fluorescence bleaching solely in the nucleus or cytosol (Dantuma et al., 2006). We transfected cells with GFP, $SOD1^{WT}$–GFP or $SOD1^{A4V}$–GFP (Fig. 4B) for 48 h, then bleached the entire nucleus and quantified the amount of relative monomeric Ub diffusing through the nuclear pore back into the nucleus (Fig. 4C). We observed a significant drop in free monomeric Ub in cells containing $SOD1^{A4V}$–GFP aggregates, but no difference in the level of monomeric Ub between cells expressing $SOD1^{WT}$ and $SOD1^{A4V}$ in the absence of inclusions (Fig. 4D).

$SOD1^{A4V}$–GFP induces changes in the ubiquitome of NSC34 cells

Free Ub exists in complex equilibrium with multiple conjugated forms, and ALS mutations may induce redistribution of Ub through altered activity in various cellular pathways. To investigate changes in the Ub-modified proteome (the 'ubiquitome') of cells expressing $SOD1^{WT}$ compared with $SOD1^{A4V}$–GFP, we performed proteomics following enrichment of cell lysates for ubiquitylated proteins (Fig. 5A). We identified 316 ubiquitylated proteins common to cells expressing either $SOD1^{WT}$ or $SOD1^{A4V}$; 55 proteins were uniquely present in the ubiquitome of cells expressing $SOD1^{A4V}$ and 11 unique proteins were identified in the ubiquitome of cells expressing $SOD1^{WT}$ (Fig. 5B; Table 1). Network analysis of known protein–protein interactions and ontology in the set of ubiquitylated proteins

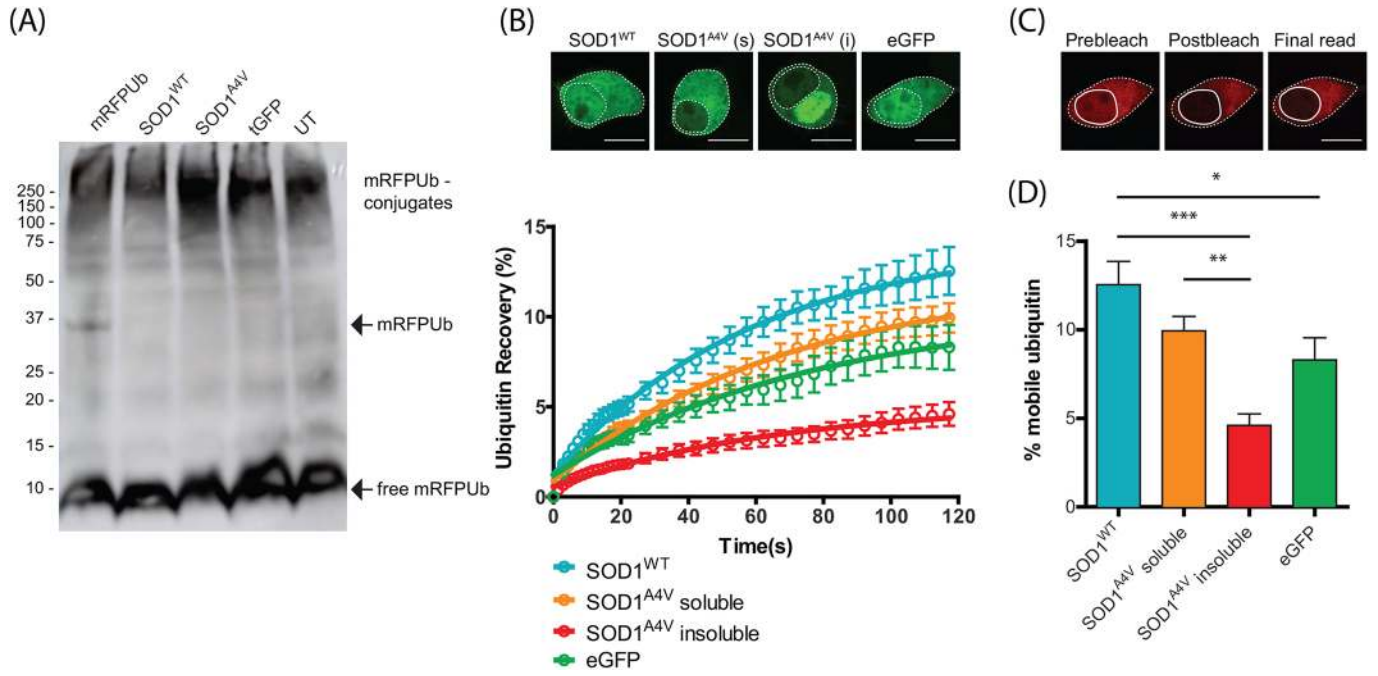

Fig. 4. Reduced levels of free monomeric Ub in NSC-34 cells containing $SOD1^{A4V}$ aggregates. (A) Western blot analysis of cell lysates of NSC-34 cells transiently transfected with $SOD1^{WT}$–GFP or $SOD1^{A4V}$–GFP, mRFP–Ub or Turbo (t)GFP control. UT, not transfected. Samples were separated under reducing conditions and probed with anti-Ub antibody. (B) The entire nucleus of co-transfected NSC-34 cells was photobleached and the recovery of nuclear Ub was monitored as a proportion of cytoplasmic fluorescence for 120 s. Data shown are means±s.e.m. ($n \geq 17$) combined from three independent experiments. Cells expressing $SOD1^{A4V}$ were classified according to whether $SOD1^{A4V}$ was either soluble (s) or insoluble (i). (C) Representative confocal images of pre-bleach, post-bleach and final read. (D) The percentage of mobile Ub in the nucleus at the final read was quantified as a proportion of cytoplasmic fluorescence. Data represent mean±s.e.m. ($n \geq 17$, combined from three independent experiments). *P<0.05; **P<0.01; ***P<0.001 (one-way ANOVA with a Tukey's comparison post test). Scale bars: 10 µm.

Journal of Cell Science (2018) 131, jcs209122. doi:10.1242/jcs.209122

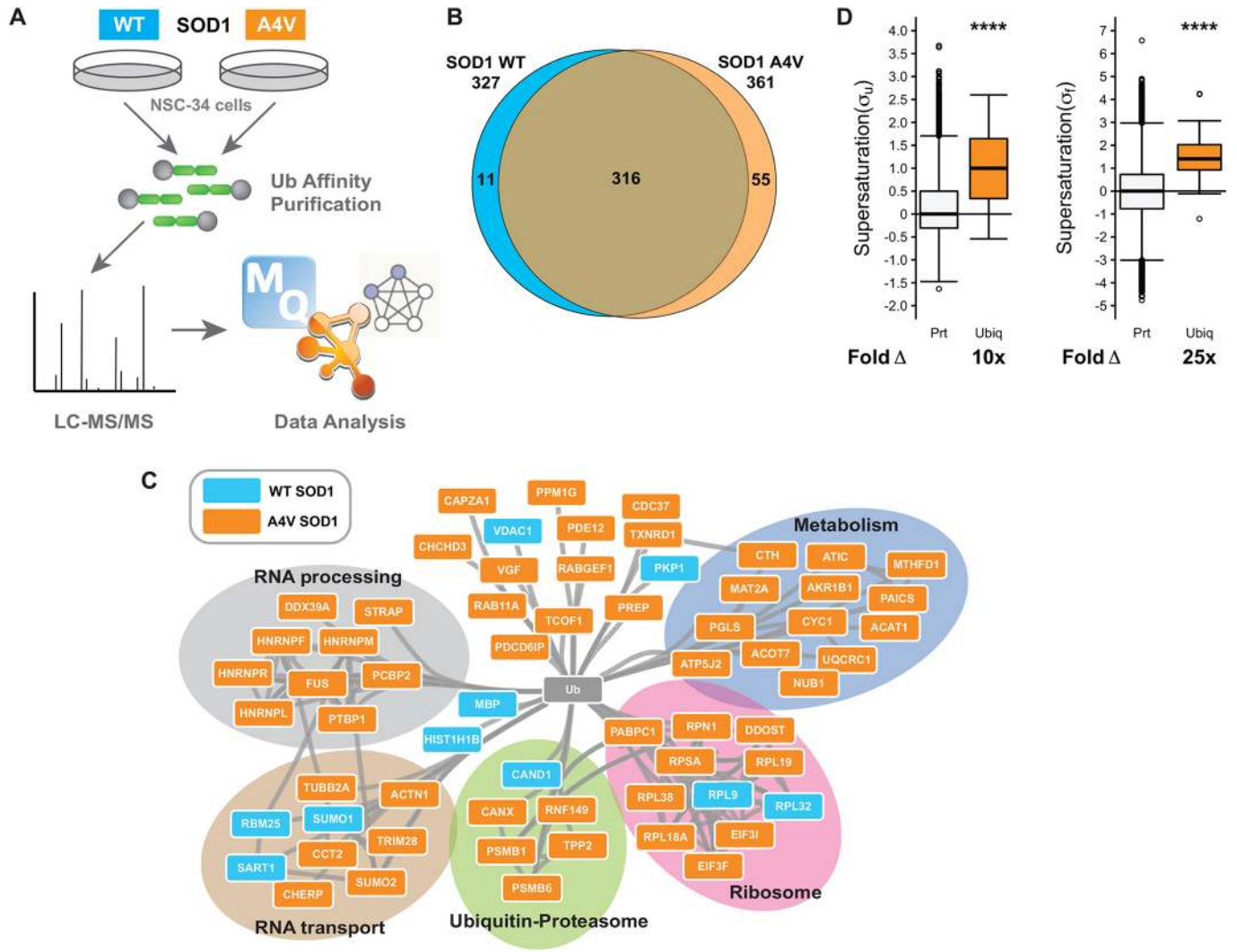

Fig. 5. The ubiquitylated proteome of transfected NSC-34 cells. (A) NSC-34 cells expressing GFP fusions of SOD1^{WT} or SOD1^{A4V} were subjected to high-affinity purification to isolate ubiquitylated proteins, which were subsequently identified by LC-MS/MS. (B) Venn analysis comparing the number of ubiquitylated proteins in NSC-34 cells transfected with either SOD1^{A4V} (*n*=2) or SOD1^{WT} (*n*=3). (C) STRING analysis of the protein–protein interaction network of ubiquitylated proteins unique to cells expressing SOD1^{A4V} or SOD1^{WT}. Proteins were identified as present in each condition if they were present in at least two replicates for that condition. Additionally proteins were only considered 'unique' to either SOD1^{WT} or SOD1^{A4V} if they were not identified in any of the replicates for any of the other conditions. (D) The median supersaturation score calculated for the unfolded (σ_u) and native (σ_f) states of proteins unique to the SOD1^{A4V} ubiquitome (Ubiq). Fold Δ refers to the increase in supersaturation score from the known mouse proteome (Prt). The box represents the 25–75th percentiles, and the median is indicated. The whiskers range from the lowest to highest value data points within 150% of the interquartile ranges. Statistical significance was assessed by the one-sided Wilcoxon/Mann–Whitney U-test with Holm–Bonferroni-corrected *P* values (****P<0.0001).

unique to cells expressing mutant SOD1^{A4V} using the String database (Szklarczyk et al., 2015) identified a number of enriched pathways, including metabolic pathways, the ubiquitin-proteasome system (UPS), and ribosome and mRNA processing and transport (Fig. 5C). Expression of a chronic misfolded protein has previously been observed to increase proteome misfolding and we have shown that ALS aggregates are composed of supersaturated proteins – that is, proteins which have expression levels higher than one might predict given their solubility (Ciryam et al., 2017).

We compared the supersaturation scores for both the unfolded and native states of ubiquitylated proteins found uniquely in SOD1^{A4V}–GFP-expressing cells to those of the whole proteome. The median supersaturation score of these 55 ubiquitylated proteins is 10× higher than that for the whole proteome in the unfolded state (σ_u) and 25× higher than that for the whole proteome in the native state (σ_f) (Fig. 5D). These data are consistent with proteome instability and resulting redeployment of Ub, driving altered Ub distribution and subsequent impairment of Ub homeostasis upon expression of a chronically misfolded protein.

Cells with SOD1^{A4V} aggregates have altered mitochondrial morphology and function

Previous work has shown that mutations in SOD1 lead to mitochondrial dysfunction (Mattiazzi et al., 2002; Vande Velde et al., 2011; Song et al., 2013; Joshi et al., 2018). Our ubiquitome analysis (above) identified enrichment of mitochondrial/metabolic proteins in the ubiquitome of SOD1^{A4V}-expressing cells (Table 1), suggesting potential mitochondrial defects in these cells. Hence, we labelled mitochondria with Mitotracker and examined morphology using confocal microscopy (Fig. 6A–C). We found that SOD1^{A4V}-expressing cells contained a significantly higher number of mitochondria per cell compared to controls (Fig. 6B). In addition,

Journal of Cell Science (2018) 131, jcs209122. doi:10.1242/jcs.209122

Table 1. Components of the ubiquitin-modified proteome (ubiquitome) identified uniquely in cells expressing either SOD1^{WT} or mutant SOD1^{A4V}

Entry	Entry name	Protein names	Gene names	Unique peptides
Unique to SOD1^{A4V}				
P14206	RSSA_MOUSE	40S ribosomal protein SA	Rpsa, Lamr1, P40-8	5
P47753	CAZA1_MOUSE	F-actin-capping protein subunit alpha-1	Capza1, Cappa1	3
Q91V12	BACH_MOUSE	Cytosolic acyl coenzyme A thioester hydrolase	Acot7, Bach	3
Q9QUR6	PPCE_MOUSE	Prolyl endopeptidase	Prep, Pep	4
Q922D8	C1TC_MOUSE	C-1-tetrahydrofolate synthase	Mthfd1	2
P45376	ALDR_MOUSE	Aldose reductase	Akr1b1, Akr1b3, Aldor1, Aldr1	4
Q8CGZ0	CHERP_MOUSE	Calcium homeostasis endoplasmic reticulum protein	Cherp, Scaf6	3
Q8R081	HNRPL_MOUSE	Heterogeneous nuclear ribonucleoprotein L	Hnrnpl, Hnrpl	2
O08784	TCOF_MOUSE	Treacle protein	Tcof1	2
O09061	PSB1_MOUSE	Proteasome subunit beta type-1	Psmb1	2
O54734	OST48_MOUSE	Dolichyl-diphosphooligosaccharide–protein glycosyltransferase 48 kDa subunit	Ddost	4
P29341	PABP1_MOUSE	Polyadenylate-binding protein 1	Pabpc1, Pabp1	4
P35564	CALX_MOUSE	Calnexin	Canx	5
P62492	RB11A_MOUSE	Ras-related protein Rab-11A	Rab11a, Rab11	2
P54729	NUB1_MOUSE	NEDD8 ultimate buster 1	Nub1, Nyren18	2
P56135	ATPK_MOUSE	ATP synthase subunit f, mitochondrial	Atp5j2	2
P56959	FUS_MOUSE	RNA-binding protein FUS	Fus	3
Q7TPR4	ACTN1_MOUSE	Alpha-actinin-1	Actn1	5
P61957	SUMO2_MOUSE	Small ubiquitin-related modifier 2	Sumo2, Smt3b, Smt3h2	2
P62717	RL18A_MOUSE	60S ribosomal protein L18a	Rpl18a	4
P80314	TCPB_MOUSE	T-complex protein 1 subunit beta	Cct2, Cctb	6
P84099	RL19_MOUSE	60S ribosomal protein L19	Rpl19	2
Q0VGU4	Q0VGU4_MOUSE	VGF nerve growth factor inducible	Vgf, mCG_18019	4
Q3THS6	METK2_MOUSE	S-adenosylmethionine synthase isoform type-2 (AdoMet synthase 2)	Mat2a	2
Q3TIU4	PDE12_MOUSE	2′,5′-phosphodiesterase 12 (2′-PDE) (2-PDE)	Pde12	2
Q3U2C5	RN149_MOUSE	E3 ubiquitin-protein ligase RNF149	Rnf149, Greul4	2
Q60692	PSB6_MOUSE	Proteasome subunit beta type-6	Psmb6, Lmp19	3
Q61074	PPM1G_MOUSE	Protein phosphatase 1G	Ppm1 g, Fin13, Ppm1c	3
Q61081	CDC37_MOUSE	Hsp90 co-chaperone Cdc37	Cdc37	2
Q61990	PCBP2_MOUSE	Poly(rC)-binding protein 2 (Alpha-CP2)	Pcbp2, Cbp, Hnrnpx, Hnrpx	2
Q62318	TIF1B_MOUSE	Transcription intermediary factor 1-beta (TIF1-beta) (E3 SUMO-protein ligase TRIM28)	Trim28, Kap1, Krip1, Tif1b	4
Q64514	TPP2_MOUSE	Tripeptidyl-peptidase 2 (TPP-2)	Tpp2	2
Q8QZT1	THIL_MOUSE	Acetyl-CoA acetyltransferase, mitochondrial	Acat1	2
Q8VCN5	CGL_MOUSE	Cystathionine gamma-lyase	Cth	3
Q8VDW0	DX39A_MOUSE	ATP-dependent RNA helicase DDX39A	Ddx39a, Ddx39	2
Q7TMK9	HNRPQ_MOUSE	Heterogeneous nuclear ribonucleoprotein Q (hnRNP Q)	Syncrip, Hnrpq, Nsap1, Nsap1l	3
Q91YQ5	RPN1_MOUSE	Dolichyl-diphosphooligosaccharide–protein glycosyltransferase subunit 1	Rpn1	5
P17225	PTBP1_MOUSE	Polypyrimidine tract-binding protein 1 (PTB)	Ptbp1, Ptb	4
Q99LX5	MMTA2_MOUSE	Multiple myeloma tumor-associated protein 2 homolog	Mmtag2	2
Q9CQ60	6PGL_MOUSE	6-phosphogluconolactonase (6PGL)	Pgls	5
Q9CRB9	MIC19_MOUSE	MICOS complex subunit Mic19	Chchd3, Mic19	3
Q9CWF2	TBB2B_MOUSE	Tubulin beta-2B chain	Tubb2b	3
Q9CWJ9	PUR9_MOUSE	Bifunctional purine biosynthesis protein PURH	Atic, Purh	4
Q9CZ13	QCR1_MOUSE	Cytochrome b-c1 complex subunit 1, mitochondrial (Complex III subunit 1)	Uqcrc1	4
Q9D0E1	HNRPM_MOUSE	Heterogeneous nuclear ribonucleoprotein M	Hnrnpm, Hnrpm	3
Q9D0M3	CY1_MOUSE	Cytochrome c1, heme protein, mitochondrial (Complex III subunit 4)	Cyc1	3
Q9DCH4	EIF3F_MOUSE	Eukaryotic translation initiation factor 3 subunit F	Eif3f, Eif3s5	4
Q9DCL9	PUR6_MOUSE	Multifunctional protein ADE2	Paics	5
Q9JJI8	RL38_MOUSE	60S ribosomal protein L38	Rpl38	3
Q9JM13	RABX5_MOUSE	Rab5 GDP/GTP exchange factor	Rabgef1, Rabex5	3
Q9JMH6	TRXR1_MOUSE	Thioredoxin reductase 1, cytoplasmic	Txnrd1, Trxr1	2
Q9QZD9	EIF3I_MOUSE	Eukaryotic translation initiation factor 3 subunit I	Eif3i, Eif3s2, Trip1	4
Q9WU78	PDC6I_MOUSE	Programmed cell death 6-interacting protein	Pdcd6ip, Aip1, Alix	4
Q9Z1Z2	STRAP_MOUSE	Serine-threonine kinase receptor-associated protein	Strap, Unrip	2
Q9Z2X1	HNRPF_MOUSE	Heterogeneous nuclear ribonucleoprotein F	Hnrnpf, Hnrpf	3
Unique to SOD1^{WT}				
B2RY56	RBM25_MOUSE	RNA-binding protein 25	Rbm25	2
P51410	RL9_MOUSE	60S ribosomal protein L9	Rpl9	5
P04370	MBP_MOUSE	Myelin basic protein	Mbp, Shi	4

Continued

Table 1. Continued

Entry	Entry name	Protein names	Gene names	Unique peptides
P43276	H15_MOUSE	Histone H1.5	Hist1h1b, H1f5	3
P62911	RL32_MOUSE	60S ribosomal protein L32	Rpl32	3
P63166	SUMO1_MOUSE	Small ubiquitin-related modifier 1 (SUMO-1)	Sumo1, Smt3c, Smt3h3, Ubl1	2
P97350	PKP1_MOUSE	Plakophilin-1	Pkp1	17
Q60932	VDAC1_MOUSE	Voltage-dependent anion-selective channel protein 1 (VDAC-1)	Vdac1, Vdac5	8
Q6ZQ38	CAND1_MOUSE	Cullin-associated NEDD8-dissociated protein 1	Cand1, D10Ertd516e, Kiaa0829	2
Q7TSF1	DSG1B_MOUSE	Desmoglein-1-beta	Dsg1b, Dsg5	6
Q9Z315	SNUT1_MOUSE	U4/U6.U5 tri-snRNP-associated protein 1	Sart1, Haf	2

these mitochondria are significantly more circular than those in control cells (Fig. 6C). We quantified Mitotracker fluorescence in cells by using flow cytometry, as above focusing on the top 10% most fluorescent cells (based on SOD1–GFP expression) to enrich for cells with aggregates (i.e. when expressing $SOD1^{A4V}$). This subset of $SOD1^{A4V}$-expressing cells has higher Mitotracker fluorescence compared to $SOD1^{WT}$-expressing cells exhibiting the same level of fluorescence – consistent with accumulation of mitochondria seen upon $SOD1^{A4V}$ expression (Fig. 6D). In the same subset of aggregate-containing cells, we observed increased fluorescence of the functional reporter CMXRos, suggesting alterations in mitochondrial membrane potential (Fig. 6E).

DISCUSSION

A unifying feature of neurodegenerative diseases such as ALS is the presence of Ub within insoluble protein aggregates (Leigh et al., 1991; Lowe et al., 1988; Mori et al., 1987). Beyond labelling substrates for degradation via the proteasome, Ub is an important regulator of cellular processes such as transcription, translation, endocytosis and DNA repair. The sequestration of Ub into inclusions may therefore reduce the availability of free Ub essential for these processes, compromising cellular function and survival. To gain insight into the regulation of Ub homeostasis in ALS, we followed the dynamic distribution of Ub at a single-cell level in a well-established SOD1 cell model of ALS. Our results confirm that the expression of mutant $SOD1^{A4V}$ leads to UPS dysfunction and corresponding disruption of Ub homeostasis, suggesting these processes plays a key role in the development of ALS pathology.

In cell models, Ub regulates the concentrations of TDP-43 and SOD1 (Scotter et al., 2014; Miyazaki et al., 2004), and proteasome inhibition can trigger their abnormal accumulation. While our previous work has established that SOD1 aggregates contain Ub

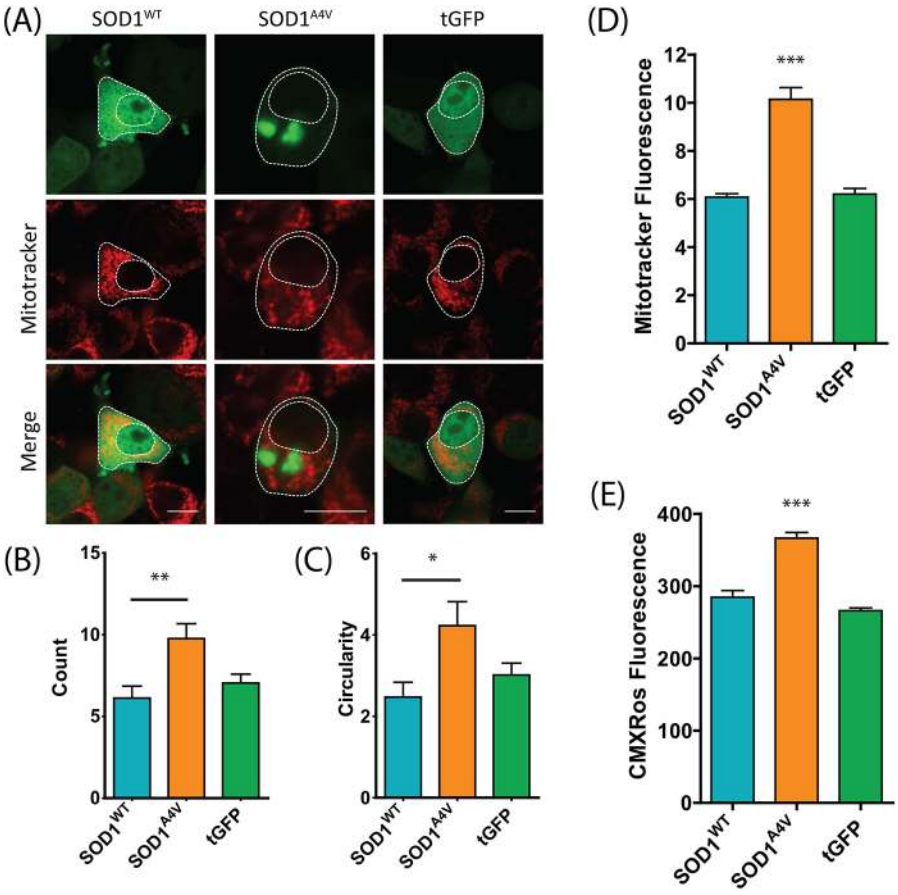

Fig. 6. Cells containing $SOD1^{A4V}$ aggregates display altered mitochondrial morphology and dysfunction. (A) NSC-34 cells transiently transfected with $SOD1^{WT}$–GFP or $SOD1^{A4V}$–GFP (or tGFP as a control) were stained for mitochondria with Mitotracker Deep Red at 48 h post transfection. Scale bars: 10 µm. The number of mitochondria (B) and their circularity (C) was determined using a mitochondrial morphology macro in ImageJ. Data represent mean±s.e.m. ($n \geq 23$). (D) Mitotracker fluorescence was also quantified by flow cytometry in cells expressing the highest levels of $SOD1^{WT}$–GFP or $SOD1^{A4V}$–GFP. (E) Mitochondrial membrane potential was examined through the accumulation of Mitotracker Red CMXRos. Data represent mean±s.e.m. ($n=3$). *$P<0.05$; **$P<0.01$; ***$P<0.001$ (one-way ANOVA with a Tukey's multiple comparison post test).

Journal of Cell Science (2018) 131, jcs209122. doi:10.1242/jcs.209122

(Farrawell et al., 2015), results here confirm that SOD1 co-aggregates with Ub, and that Ub is present at the earliest stage of aggregation. Furthermore, SOD1 aggregates were found to contain both K48- and K63-linked polyubiquitin chains, which signal degradation via the proteasome and autophagy pathways, respectively (Kwon and Ciechanover, 2017). Interestingly, both K48- and K63-linked ubiquitylation has been associated with the formation of inclusions (Tan et al., 2008), with previous studies showing that K63 polyubiquitylation directs misfolded SOD1 to the ubiquitin-aggresome route when the UPS is inhibited (Wang et al., 2012). These data are consistent with the need for tightly regulated Ub homeostasis in neurons, and suggest that any perturbation in this homeostasis could cause Ub depletion and subsequent toxicity. It is likely that protein aggregation causes Ub depletion, which could then drive further aggregation in a positive-feedback loop (Fig. 7).

In the nervous system, the UPS contributes to the regulation of many aspects of synaptic function, such as neuronal growth and development, neuronal excitability, neurotransmission, long-term potentiation (LTP) and synapse formation and elimination (Mabb and Ehlers, 2010; Kawabe and Brose, 2011). UPS dysfunction is therefore central to neuronal health and neurodegenerative disease (Yerbury et al., 2016). Impairment of the UPS has been implicated strongly in the pathogenesis of ALS (Scotter et al., 2014; Tashiro et al., 2012; Cheroni et al., 2009). Here, we reveal that the aggregation of SOD1 compromises UPS function, decreasing cellular capacity to degrade the proteasome reporter tdTomato^{CL1}. Our findings are consistent with the previous demonstration of UPS dysfunction in ALS, with accumulation of the fluorescent UPS reporter Ub^{G76V}–GFP observed in the spinal cord and cranial motor neurons of SOD1^{G93A} mice (Cheroni et al., 2009). Moreover, a motor neuron-specific knockdown of the proteasome subunit Rpt3 in the absence of ALS genetic background results in an ALS phenotype in mice – including locomotor dysfunction, progressive motor neuron loss and mislocalisation of ALS markers TDP-43, FUS, ubiquilin 2 and optineurin (Tashiro et al., 2012). These data support a model where a reduction in UPS capacity is sufficient to drive ALS pathology in mice. Not even overexpression of human mutant TDP-43 gives such an accurate reproduction of a human ALS-like phenotype in mice. In ALS patient spinal motor neurons, 85% (38/40) of cytoplasmic TDP-43 foci or inclusions were positive for Ub. In fact, almost all cellular Ub in these neurons was sequestered within large skein-like inclusions (Farrawell et al., 2015). Interestingly, Ub has been found to accumulate in inclusions without the aggregation of TDP-43 in sALS (Giordana et al., 2010), suggesting that aggregation of proteins, such as TDP-43, FUS and SOD1 may not be necessary for Ub depletion-induced toxicity. In human skin fibroblasts, it has been shown that the UPS reporter GFP^{CL1} accumulates significantly more in ALS patient fibroblasts compared to controls, suggesting a compromised UPS (Yang et al., 2015). This raises the question of whether there are alternative means to control protein concentration when protein aggregates disrupt degradation mechanisms. It was recently proposed that

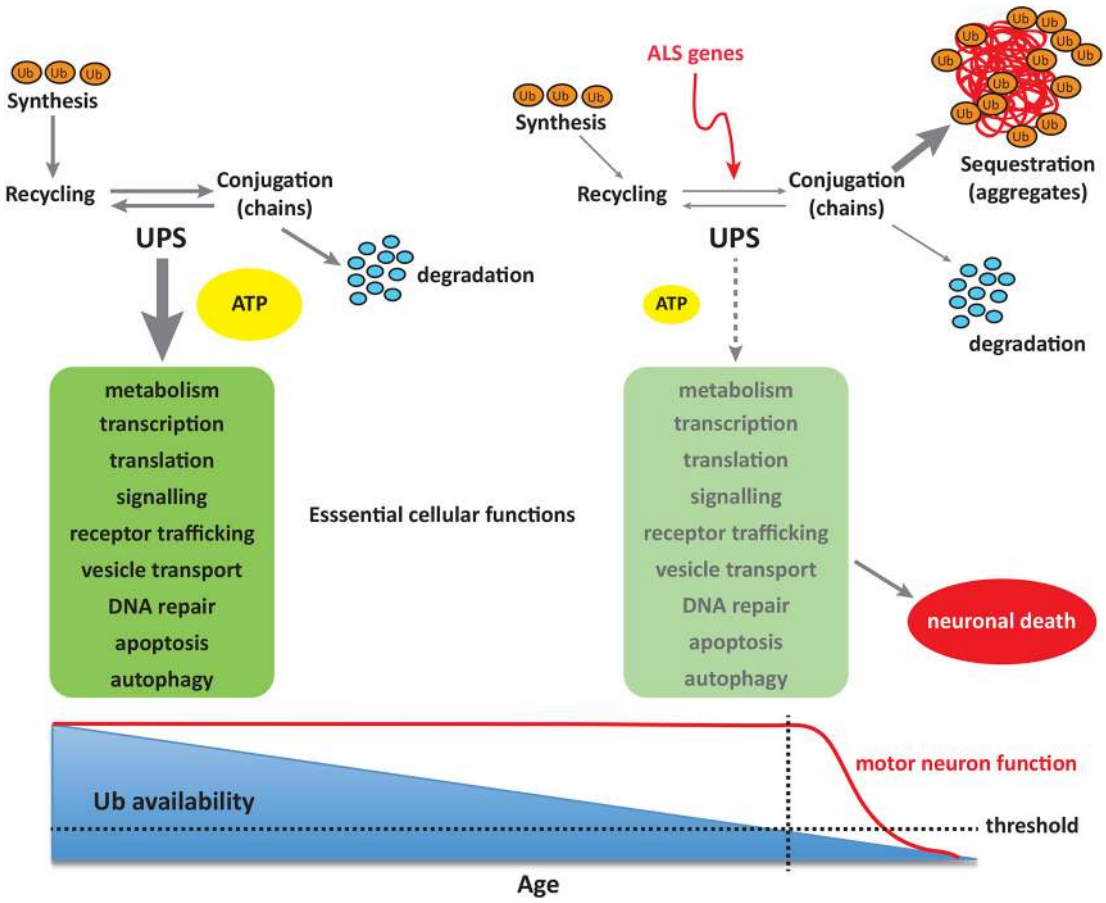

Fig. 7. Disrupted Ub homeostasis in ALS. Mutations in SOD1-associated ALS disrupt Ub homeostasis, either directly or through sequestration of Ub into protein aggregates. These changes result in altered Ub distribution and subsequent depletion of free Ub, eventually reaching a threshold below which vital cellular functions are severely compromised, and ultimately result in cell death.

widespread transcriptional repression may serve this purpose in Alzheimer's disease (Ciryam et al., 2016).

The work presented here suggests that the aggregation of misfolded SOD1 alters Ub homeostasis and subsequently depletes the free Ub pool in cells. Cellular Ub exists in a complex equilibrium between free and conjugated Ub (Dantuma et al., 2006). Neurons are vulnerable to a deficiency in free Ub, which, if prolonged, can lead to cell death (Tan et al., 2000, 2001). Many factors can influence Ub homeostasis. For example, proteasome inhibition depletes free Ub to as low as 5% of basal levels in less than 2 h (Mimnaugh et al., 1997; Patnaik et al., 2000). Inhibition of translation also depletes free Ub through reduced production, while toxicity can be rescued by overexpression of Ub (Hanna et al., 2003). Accumulation of ubiquitylated proteins in inclusions is an important potential mechanism for depletion of free Ub, and, in this context, free Ub levels can be partially restored by overexpression or removal of Ub from the aggregated protein through ubiquitin-specific proteases. It was recently shown that while the ataxia-associated mutation in Usp14 causes a reduction in free Ub and neuromuscular junction dysfunction in mice, overexpression of Ub restored free Ub levels in motor neurons and improved the neuromuscular junction (NMJ) structure (Vaden et al., 2015). Additionally, free Ub could be increased in cells containing huntingtin aggregates by overexpression of the de-ubiquitylation enzyme USP14 (Hyrskyluoto et al., 2014). Not only did this protect cells from aggregate-induced toxicity, it also reduced ER stress, which is thought to precede inclusion formation in ALS models (Atkin et al., 2014). Furthermore, perturbations in ubiquitin homeostasis caused by dysregulation of ubiquitin-like modifier activating enzyme 1 (UBA1) induces neuromuscular pathology in animal models of spinal muscular atrophy (Wishart et al., 2014; Powis et al., 2016). Systemic restoration of UBA1 has been shown to rescue this pathology (Powis et al., 2016). These data further support the concept that modulation of cellular Ub pools is an important factor in the pathogenesis of neurodegenerative disease.

The pathways responsible for modulating Ub homeostasis in ALS are not yet well understood. Our ubiquitomics analysis of cells expressing SOD1 reveals that the unique ubiquitome of cells expressing $SOD1^{A4V}$ is enriched for proteins prone to aggregation (i.e. that are supersaturated). This is consistent with findings that proteins associated with neurodegeneration are supersaturated (Ciryam et al., 2013, 2015, 2017). Furthermore, a substantial proportion of the ubiquitylated proteins identified are from pathways known to be dysfunctional in ALS, including RNA processing, and metabolic and mitochondrial pathways. This is not surprising given that both RNA-binding proteins and oxidative phosphorylation and metabolic pathways are also prone to aggregation in neurodegeneration (Ciryam et al., 2015). These results suggest that mutations in SOD1 may lead to mitochondrial dysfunction by disrupting Ub homeostasis. Interestingly, we find that cells expressing mutant $SOD1^{A4V}$ had altered mitochondrial morphology and function. Disturbances to mitochondrial morphology and function have been previously reported in human motor neurons carrying the $SOD1^{A4V}$ mutation (Kiskinis et al., 2014) and NSC-34 cells expressing mutant $SOD1^{G93A}$ (Joshi et al., 2018). Recent studies have revealed that mitochondrial impairment occurs soon after proteasome inhibition (Maharjan et al., 2014). In fact, continued proteasome dysfunction in mouse brain cortical neurons inhibited the degradation of ubiquitylated mitochondrial proteins and led to the accumulation of dysfunctional mitochondria (Ugun-Klusek et al., 2017). Misfolded proteins such as mutant SOD1 have also been shown to interact with mitochondrial proteins and translocate into the mitochondrial intermembrane space and mitochondrial matrix, where they accumulate and induce mitochondrial dysfunction (Vijayvergiya et al., 2005; Jaarsma et al., 2001; Ruan et al., 2017; Igoudjil et al., 2011; Fischer et al., 2011). However, this cytotoxicity can be attenuated through the ubiquitylation of misfolded but non-aggregated SOD1, which promotes its degradation via the UPS (Yonashiro et al., 2009). Collectively, these studies demonstrate an integral functional relationship between impairment of the UPS and mitochondrial dysfunction, and that modulation of cellular Ub pools may rescue mitochondrial dysfunction caused by the accumulation of SOD1.

Conclusions

In conclusion, we observe that the aggregation of mutant $SOD1^{A4V}$ leads to altered UPS activity and redistribution of Ub, causing disrupted Ub homeostasis. Given that Ub controls many essential cellular pathways that are also dysfunctional in ALS – including transcription, translation, vesicle transport, mitochondrial function and apoptosis – these findings suggest that Ub homeostasis is a central feature of ALS pathogenesis. Further understanding of the contribution of Ub homeostasis to ALS pathology may be imperative to understanding the molecular pathways underpinning neurodegenerative disease more broadly.

MATERIALS AND METHODS

Plasmids

pEGFP-N1 vectors containing human $SOD1^{WT}$ and $SOD1^{A4V}$ were generated as described previously (Turner et al., 2005). The tGFP construct (pCMV6-AC-GFP) was obtained from OriGene (USA). GFP–Ub and mRFP–Ub (Addgene plasmids 11928 and 11935, deposited by Nico Dantuma; Dantuma et al., 2006; Bergink et al., 2006) were acquired from Addgene. The mCherry–Ub construct was created by replacing the mRFP sequence in mRFP–Ub with mCherry fluorescent protein. The $tdTomato^{CL1}$ construct was obtained by cloning the CL1 sequence (ACKNWFSSLSHFVIHL) into pcDNA3.1(+)tdTomato.

Cell culture and transfection

Neuroblastoma×spinal cord hybrid NSC-34 cells (Cashman et al., 1992) were maintained in Dulbecco's Modified Eagle's Medium/Ham's Nutrient Mixture F12 (DMEM/F12) supplemented with 10% fetal bovine serum (FBS, Bovogen Biologicals, Australia). Cells were maintained at 37°C in a humidified incubator with 5% atmospheric CO_2. For confocal microscopy, cells were grown on 13 mm round coverslips in 24-well plates or on eight-well µ-slides (Ibidi, Germany). Cells were grown in six-well plates for cell lysate and cell sorting experiments. Cells were transfected using Lipofectamine 3000 (Invitrogen, USA) according to manufacturer's instructions with 0.5 µg DNA per well for a 24-well plate, 0.2 µg DNA per well for eight-well µ-slides and 2.5 µg DNA per well for six-well plates. For co-transfections the amount of DNA was divided equally between constructs. Animal studies were performed with the approval (AE11/29 and AE12/09) of the Animal Ethics Committee of the University of Wollongong (Wollongong, Australia).

Measurement of UPS function

To quantify UPS activity, NSC-34 cells were co-transfected with the fluorescent proteasome reporter $tdTomato^{CL1}$ and treated overnight (~18 h) with 0–30 µM of the proteasome inhibitor MG132. The level of $tdTomato^{CL1}$ fluorescence was determined via flow cytometry on a Becton Dickinson flow cytometer 48 h post transfection as in Yang et al. (2015).

Live cell imaging

Imaging of NSC-34 cells co-transfected with $SOD1^{A4V}$–GFP and mRFP–Ub was performed 24 h post transfection on a Leica TCS SP5 confocal microscope. Cells were imaged every 15 min over 17 h in a CO_2 chamber maintained at 37°C with 5% CO_2. For fluorescence recovery after photobleaching (FRAP) and fluorescence recovery after nucleus photobleaching (FRANP) experiments, analysis was performed on

transfected NSC-34 cells at 48 h post transfection using the LAS AF FRAP Application Wizard on the Leica TCS SP5 confocal microscope. Images were acquired using the 63× objective with two line averages and a scan speed of 700 Hz. Five pre-bleach images were acquired over 7.5 s with the 561 nm laser set at 20% power. The region of interest (ROI) was then bleached using the 'zoom in ROI' method over five frames of 1.5 s at 100% laser power. For FRANP analysis, the entire nucleus was bleached. Fluorescence recovery or loss was monitored for 120 s with the laser power set back at 20%.

To quantify SOD1 inclusion formation, images were acquired as described previously (McAlary et al., 2016). Briefly, *z*-stack images of NSC-34 cells transfected with SOD1–GFP constructs were acquired at 48 h post transfection using the 63× objective, 512×512 pixels, one line and frame average, and a scan speed of 400 Hz. *z*-stacks were processed into a single image using LAS-AF Lite software (Leica) and at least 100 transfected cells were analysed for the presence of inclusions.

Frequency distribution analysis

GFP fluorescence in NSC-34 cells expressing soluble and insoluble (aggregated) SOD1^{A4V}–GFP was quantified from confocal images taken 48 h post transfection using ImageJ 1.48v (Schneider et al., 2012). A minimum of 100 transfected cells were analysed per experiment. Frequency distribution analysis was subsequently performed in GraphPad Prism version 5.00 for Windows (GraphPad software, USA).

Toxicity assay

The viability of cells expressing SOD1 was monitored over 68 h in an Incucyte automated fluorescent microscope (Essen BioScience, USA) as described in McAlary et al. (2016). Cells were dissociated at 24 h post transfection and re-plated in 96-well plates at a confluency of 20% in Phenol-Red-free DMEM/F12 containing 10% FBS. Images were acquired every 2 h and analysed using a processing definition trained to select GFP-positive cells. The number of GFP-positive cells was normalised to time zero before SOD1^{A4V} numbers were normalised to SOD1^{WT} values.

Immunofluorescence

NSC-34 cells grown on coverslips were transfected with GFP-tagged SOD1^{A4V} and fixed for 20 min at room temperature (RT) with 4% paraformaldehyde (PFA) (Merck Millipore, USA) in phosphate-buffered saline (PBS) 48 h post transfection. Cells were permeabilised in 1% Triton X-100 (TX-100) in PBS for 30 min on ice before blocking for 1 h at RT with 5% FBS, 1% bovine serum albumin (BSA) 0.3% TX-100 in PBS. Cells were incubated with rabbit primary antibodies against K48 or K63 Ub chain linkages (05-1307/05-1308, Merck Millipore; 1:500 dilution) overnight at 4°C followed by Alexa Fluor 647-conjugated anti-rabbit-IgG secondary antibody (ab150079, Abcam, UK; 1:500 dilution) for 5 h at RT. All antibodies were diluted in 1% BSA, 0.1% TX-100 in PBS and cells were washed with PBS between each incubation step.

Spinal cord sections from the SOD1^{G93A} mouse were also stained for SOD1 and K48 or K63 Ub chain linkages. A pap pen (Daido Sangyo, Tokyo, Japan) was used to separate tissue sections mounted onto the same slide. Sections were then fixed with 4% PFA for 15 min at RT before permeabilisation at RT for 10 min with 0.1% TX-100 in PBS containing 2% (v/v) normal horse serum (NHS). Sections were then blocked for 20 min at RT with 20% NHS and 2% BSA in PBS followed by staining overnight at 4°C in a humidified chamber with sheep anti-SOD1 (ab8866, Abcam; 1:200 dilution), mouse neuron-specific βIII tubulin antibody (ab78078, Abcam; 1:200 dilution) and rabbit anti-ubiquitin K48 or K63 (Merck Millipore; 1:200 dilution). The following day, sections were incubated with 4 µg/ml Alexa Fluor-conjugated secondary antibodies reactive to sheep, mouse and rabbit IgG (A21100, Invitrogen; ab150114, Abcam; A181448, Invitrogen) for 1 h at RT. Following staining, coverslips were mounted onto slides using ProLong Diamond Antifade Mountant (Molecular Probes). All imaging experiments were performed on a Leica TCS SP5 confocal microscope.

Cell lysis

NSC-34 cells grown in six-well plates and transfected with SOD1–GFP or mRFP–Ub were harvested 48 h post transfection with trypsin-EDTA (Gibco). Cells were washed with PBS before being resuspended in RIPA buffer [50 mM Tris-HCl pH 7.4, 1% (w/v) sodium deoxycholate, 150 mM NaCl, 1 mM EDTA, 1% TX-100, 0.1% SDS, 10 mM NEM, 1 mM sodium orthovanadate, Halt™ Protease Inhibitor Cocktail (Thermo Scientific)]. Protein concentration was determined with a BCA assay.

Western blotting

Cell lysates with a total protein concentration of 100 µg were reduced with β-mercaptoethanol and heated for 10 min at 70°C before being analysed on a Mini-PROTEAN TGX Stain-Free Gel (Bio-Rad) for 2 h at 100 V. Proteins were transferred onto a nitrocellulose membrane (Pall Corporation) using the standard protocol on the Bio-Rad Trans-Blot Turbo Transfer System. The membrane was blocked in 5% skim milk powder in Tris-buffered saline with 0.2% (v/v) Tween-20 (TBST) for 1 h at RT before probing for Ub with rabbit anti-Ub antibody (ab137025, Abcam; 1:1500 dilution) overnight at 4°C. The following day the membrane was washed three times with TBST over 30 min before incubating with horseradish peroxidise (HRP)-conjugated anti-rabbit-IgG antibody (1706515, Bio-Rad; 1:2000 dilution) for 1 h at RT. The membrane was visualised with chemiluminescent substrate (Thermo Scientific) on the Amersham Imager 6600RGB.

Cell sorting

NSC-34 cells transfected with SOD1^{WT}-GFP or SOD1^{A4V}–GFP were harvested 24 h post transfection with trypsin-EDTA (Gibco) and washed with PBS before being resuspended in Phenol Red-free medium containing 10% FBS and filtered through a 35 µm nylon mesh strainer (Greiner Bio-One, Austria). Enrichment of GFP-positive cells was performed on a FACS Aria III (BD Biosciences, USA) and a BD FACs Aria II (BD Biosciences). Cells were sorted based on GFP fluorescence (excitation 488 nm, emission 530/30 nm) and collected into 5 ml FACS tubes containing 1 ml FBS. Following enrichment, cells were lysed for ubiquitomics analysis.

Ubiquitomics

Proteomics to identify the ubiquitin-modified proteome (the 'ubiquitome') in NSC-34 cells was performed as described in Nagarajan et al. (2017). Cells were lysed in lysis buffer (50 mM Tris-HCl pH 7.5, 150 mM NaCl, 0.5% NP-40, 1 mM DTT, 1× EDTA-free protease inhibitor cocktail, 10 mM N-ethylmaleimide, 1 mM sodium orthovanadate). Protein concentration was determined using a BCA assay, and 300 µg of total protein was used per sample to immunopurify mono- and poly-ubiquitylated proteins using 30 µl of VIVAbind Ub affinity matrix (Ubiquitin Kit, VIVA Bioscience). Samples were incubated for 2 h at 4°C with end-to-end mixing then matrix was collected by centrifugation (1 min; 4°C; 1000 ***g***) and washed six times in 500 µl of detergent-free wash buffer [50 mM Tris-HCl (pH 7.5), 150 mM NaCl, 1 mM DTT, 1x EDTA-free protease inhibitor cocktail, 10 mM N-ethylmaleimide, 1 mM sodium orthovanadate]. After washing, beads were digested for 30 min at 27°C, then reduced with 1 mM DTT and left to digest overnight at RT with sequencing-grade trypsin (5 µg/ml, Promega), as described previously (Turriziani et al., 2014). Samples were alkylated with 5 mg/ml iodoacetamide, and protease digestion terminated with trifluoroacetic acid. Trypsinised eluents were collected after a brief centrifugation then purified and desalted using self-packed tips with six layers of C18 Empore disks (Pacific Laboratory Products), then dried in a SpeedVac. Samples were then resuspended in 12 µl 5% formic acid, 2% acetonitrile and stored at −80°C.

For nano-liquid chromatography tandem mass spectrometry (nLC-MS/MS) analysis, 5 µl of each of the peptide samples were loaded and separated along a C18 column (400 mm, 75 µm ID, 3 µm silica beads) and introduced by nanoelectrospray into an LTQ Orbitrap Velos Pro coupled to an Easy-nLC HPLC (Thermo Fisher). MS/MS data were collected for the top ten most abundant ions per scan over a 140-min time gradient. The order of data collection was randomised to interchange between biological conditions with BSA run between each sample to minimise temporal bias. MS/MS raw files were analysed using the Andromeda search engine integrated into MaxQuant (v1.2.7.4) (Cox and Mann, 2008) against the Uniprot Mouse database. A false discovery rate of 1% was tolerated for protein, peptide and sites, and one missed cleavage was allowed. MaxQuant output data were filtered to remove contaminants, reverse hits, proteins only identified by site and proteins with <2 unique peptides (Croucher et al., 2016). An individual protein was defined as present under a particular condition if it was detected

in a minimum of two replicates. Protein–protein interactions and KEGG pathway analysis among the resulting protein list was analysed using STRING (v10) (Szklarczyk et al., 2015) (with a confidence score of 0.700) and Cytoscape (v3.1.1) (Smoot et al., 2011).

Analysis of mitochondrial morphology and function

NSC-34 cells transiently transfected with $SOD1^{WT}$-GFP or $SOD1^{A4V}$–GFP were incubated with 100 nM Mitotracker Deep Red FM (Molecular Probes) or Mitotracker CMXRos (Molecular Probes) for 30 min at 37°C prior to analysis by confocal microscopy or flow cytometry at 48 h post transfection. Mitochondrial morphology was examined with a mitochondrial morphology macro (Dagda et al., 2009) on ImageJ 1.48v. Mitotracker Red and Mitotracker CMXRos accumulation in cells expressing high levels of SOD1–GFP was also assessed by flow cytometry (Becton Dickinson).

Acknowledgements

The authors would like to gratefully acknowledge Clare Watson who helped with editing and proof reading the manuscript.

Competing interests

The authors declare no competing or financial interests.

Author contributions

Conceptualization: N.E.F., D.N.S., J.J.Y.; Methodology: N.E.F., I.L.-S., J.M., L.M., K.L.V., D.N.S., J.J.Y.; Validation: I.L.-S.; Formal analysis: K.M., J.M., P.C., K.L.V., D.N.S., J.J.Y.; Investigation: P.C., J.J.Y.; Resources: D.N.S., J.J.Y.; Data curation: N.E.F., K.M., L.M., P.C.; Writing - original draft: N.E.F., J.J.Y.; Writing - review & editing: N.E.F., I.L.-S., L.M., P.C., K.L.V., D.N.S., J.J.Y.; Visualization: N.E.F.; Supervision: K.L.V., D.N.S., J.J.Y.; Project administration: K.L.V., J.J.Y.; Funding acquisition: K.L.V., D.N.S., J.J.Y.

Funding

I.L.-S. was supported by Australian Rotary Health. P.C. was supported by grants from the US-UK Fulbright Commission, St John's College, University of Cambridge, and the National Institutes of Health (Northwestern University Medical Scientist Training Program Grant T32 GM8152-28). D.N.S., K.L.V. and J.J.Y. were supported by US Department of Defense (AL150057) and the Motor Neuron Disease Research Institute of Australia (Cunningham Family MND research grant, GIA1656). J.J.Y. was also supported by grants from the National Health and Medical Research Council (1095215, 1084144). Deposited in PMC for release after 12 months.

Data availability

The datasets used and/or analysed during the current study are available from the corresponding author on reasonable request.

Supplementary information

Supplementary information available online at
http://jcs.biologists.org/lookup/doi/10.1242/jcs.209122.supplemental

References

Atkin, J. D., Farg, M. A., Soo, K. Y., Walker, A. K., Halloran, M., Turner, B. J., Nagley, P. and Horne, M. K. (2014). Mutant SOD1 inhibits ER-Golgi transport in amyotrophic lateral sclerosis. *J. Neurochem.* **129**, 190-204.

Bence, N. F., Sampat, R. M. and Kopito, R. R. (2001). Impairment of the ubiquitin-proteasome system by protein aggregation. *Science* **292**, 1552-1555.

Bergink, S., Salomons, F. A., Hoogstraten, D., Groothuis, T. A., de Waard, H., Wu, J., Yuan, L., Citterio, E., Houtsmuller, A. B., Neefjes, J. et al. (2006). DNA damage triggers nucleotide excision repair-dependent monoubiquitylation of histone H2A. *Genes Dev.* **20**, 1343-1352.

Boeynaems, S., Bogaert, E., Kovacs, D., Konijnenberg, A., Timmerman, E., Volkov, A., Guharoy, M., De Decker, M., Jaspers, T., Ryan, V. H. et al. (2017). Phase separation of C9orf72 dipeptide repeats perturbs stress granule dynamics. *Mol. Cell* **65**, 1044-1055 e5.

Brettschneider, J., Arai, K., Del Tredici, K., Toledo, J. B., Robinson, J. L., Lee, E. B., Kuwabara, S., Shibuya, K., Irwin, D. J., Fang, L. et al. (2014). TDP-43 pathology and neuronal loss in amyotrophic lateral sclerosis spinal cord. *Acta Neuropathol.* **128**, 423-437.

Cashman, N. R., Durham, H. D., Blusztajn, J. K., Oda, K., Tabira, T., Shaw, I. T., Dahrouge, S. and Antel, J. P. (1992). Neuroblastoma x spinal cord (NSC) hybrid cell lines resemble developing motor neurons. *Dev. Dyn.* **194**, 209-221.

Chen, S., Sayana, P., Zhang, X. and Le, W. (2013). Genetics of amyotrophic lateral sclerosis: an update. *Mol. Neurodegener* **8**, 28.

Cheroni, C., Marino, M., Tortarolo, M., Veglianese, P., De Biasi, S., Fontana, E., Zuccarello, L. V., Maynard, C. J., Dantuma, N. P. and Bendotti, C. (2009). Functional alterations of the ubiquitin-proteasome system in motor neurons of a mouse model of familial amyotrophic lateral sclerosis. *Hum. Mol. Genet.* **18**, 82-96.

Chiti, F. and Dobson, C. M. (2006). Protein misfolding, functional amyloid, and human disease. *Annu. Rev. Biochem.* **75**, 333-366.

Ciechanover, A. and Brundin, P. (2003). The ubiquitin proteasome system in neurodegenerative diseases: sometimes the chicken, sometimes the egg. *Neuron* **40**, 427-446.

Cirulli, E. T., Lasseigne, B. N., Petrovski, S., Sapp, P. C., Dion, P. A., Leblond, C. S., Couthouis, J., Lu, Y. F., Wang, Q., Krueger, B. J. et al. (2015). Exome sequencing in amyotrophic lateral sclerosis identifies risk genes and pathways. *Science* **347**, 1436-1441.

Ciryam, P., Tartaglia, G. G., Morimoto, R. I., Dobson, C. M. and Vendruscolo, M. (2013). Widespread aggregation and neurodegenerative diseases are associated with supersaturated proteins. *Cell Rep.* **5**, 781-790.

Ciryam, P., Kundra, R., Morimoto, R. I., Dobson, C. M. and Vendruscolo, M. (2015). Supersaturation is a major driving force for protein aggregation in neurodegenerative diseases. *Trends Pharmacol. Sci.* **36**, 72-77.

Ciryam, P., Kundra, R., Freer, R., Morimoto, R. I., Dobson, C. M. and Vendruscolo, M. (2016). A transcriptional signature of Alzheimer's disease is associated with a metastable subproteome at risk for aggregation. *Proc. Natl. Acad. Sci. USA* **113**, 4753-4758.

Ciryam, P., Lambert-Smith, I. A., Bean, D. M., Freer, R., Cid, F., Tartaglia, G. G., Saunders, D. N., Wilson, M. R., Oliver, S. G., Morimoto, R. I. et al. (2017). Spinal motor neuron protein supersaturation patterns are associated with inclusion body formation in ALS. *Proc. Natl. Acad. Sci. USA* **114**, E3935-E3943.

Cox, J. and Mann, M. (2008). MaxQuant enables high peptide identification rates, individualized p.p.b.-range mass accuracies and proteome-wide protein quantification. *Nat. Biotechnol.* **26**, 1367-1372.

Croucher, D. R., Iconomou, M., Hastings, J. F., Kennedy, S. P., Han, J. Z., Shearer, R. F., McKenna, J., Wan, A., Lau, J., Aparicio, S. et al. (2016). Bimolecular complementation affinity purification (BiCAP) reveals dimer-specific protein interactions for ERBB2 dimers. *Sci. Signal.* **9**, ra69.

Dagda, R. K., Cherra, S. J., III, Kulich, S. M., Tandon, A., Park, D. and Chu, C. T. (2009). Loss of PINK1 function promotes mitophagy through effects on oxidative stress and mitochondrial fission. *J. Biol. Chem.* **284**, 13843-13855.

Dantuma, N. P., Groothuis, T. A., Salomons, F. A. and Neefjes, J. (2006). A dynamic ubiquitin equilibrium couples proteasomal activity to chromatin remodeling. *J. Cell Biol.* **173**, 19-26.

Farrawell, N. E., Lambert-Smith, I. A., Warraich, S. T., Blair, I. P., Saunders, D. N., Hatters, D. M. and Yerbury, J. J. (2015). Distinct partitioning of ALS associated TDP-43, FUS and SOD1 mutants into cellular inclusions. *Sci. Rep.* **5**, 13416.

Fischer, L. R., Igoudjil, A., Magrané, J., Li, Y., Hansen, J. M., Manfredi, G. and Glass, J. D. (2011). SOD1 targeted to the mitochondrial intermembrane space prevents motor neuropathy in the Sod1 knockout mouse. *Brain* **134**, 196-209.

Giordana, M. T., Piccinini, M., Grifoni, S., De Marco, G., Vercellino, M., Magistrello, M., Pellerino, A., Buccinna, B., Lupino, E. and Rinaudo, M. T. (2010). TDP-43 redistribution is an early event in sporadic amyotrophic lateral sclerosis. *Brain Pathol.* **20**, 351-360.

Grad, L. I., Yerbury, J. J., Turner, B. J., Guest, W. C., Pokrishevsky, E., O'Neill, M. A., Yanai, A., Silverman, J. M., Zeineddine, R., Corcoran, L. et al. (2014). Intercellular propagated misfolding of wild-type Cu/Zn superoxide dismutase occurs via exosome-dependent and -independent mechanisms. *Proc. Natl. Acad. Sci. USA* **111**, 3620-3625.

Groothuis, T. A., Dantuma, N. P., Neefjes, J. and Salomons, F. A. (2006). Ubiquitin crosstalk connecting cellular processes. *Cell Div.* **1**, 21.

Hanna, J., Leggett, D. S. and Finley, D. (2003). Ubiquitin depletion as a key mediator of toxicity by translational inhibitors. *Mol. Cell. Biol.* **23**, 9251-9261.

Hershko, A. and Ciechanover, A. (1998). The ubiquitin system. *Annu. Rev. Biochem.* **67**, 425-479.

Huang, Q. and Figueiredo-Pereira, M. E. (2010). Ubiquitin/proteasome pathway impairment in neurodegeneration: therapeutic implications. *Apoptosis* **15**, 1292-1311.

Hyrskyluoto, A., Bruelle, C., Lundh, S. H., Do, H. T., Kivinen, J., Rappou, E., Reijonen, S., Waltimo, T., Petersen, A., Lindholm, D. et al. (2014). Ubiquitin-specific protease-14 reduces cellular aggregates and protects against mutant huntingtin-induced cell degeneration: involvement of the proteasome and ER stress-activated kinase IRE1alpha. *Hum. Mol. Genet.* **23**, 5928-5939.

Igoudjil, A., Magrane, J., Fischer, L. R., Kim, H. J., Hervias, I., Dumont, M., Cortez, C., Glass, J. D., Starkov, A. A. and Manfredi, G. (2011). In vivo pathogenic role of mutant SOD1 localized in the mitochondrial intermembrane space. *J. Neurosci.* **31**, 15826-15837.

Jaarsma, D., Rognoni, F., van Duijn, W., Verspaget, H. W., Haasdijk, E. D. and Holstege, J. C. (2001). CuZn superoxide dismutase (SOD1) accumulates in vacuolated mitochondria in transgenic mice expressing amyotrophic lateral sclerosis-linked SOD1 mutations. *Acta Neuropathol.* **102**, 293-305.

Joshi, A. U., Saw, N. L., Vogel, H., Cunnigham, A. D., Shamloo, M. and Mochly-Rosen, D. (2018). Inhibition of Drp1/Fis1 interaction slows progression of amyotrophic lateral sclerosis. *EMBO Mol. Med.* **10**, e8166.

Kawabe, H. and Brose, N. (2011). The role of ubiquitylation in nerve cell development. *Nat. Rev. Neurosci.* **12**, 251-268.
Kiskinis, E., Sandoe, J., Williams, L. A., Boulting, G. L., Moccia, R., Wainger, B. J., Han, S., Peng, T., Thams, S., Mikkilineni, S. et al. (2014). Pathways disrupted in human ALS motor neurons identified through genetic correction of mutant SOD1. *Cell Stem Cell* **14**, 781-795.
Kwon, Y.T. and Ciechanover, A. (2017). The Ubiquitin Code in the Ubiquitin-Proteasome System and Autophagy. *Trends Biochem Sci.* **42**(11), 873-886.
Leigh, P. N., Whitwell, H., Garofalo, O., Buller, J., Swash, M., Martin, J. E., Gallo, J. M., Weller, R. O. and Anderton, B. H. (1991). Ubiquitin-immunoreactive intraneuronal inclusions in amyotrophic lateral sclerosis. Morphology, distribution, and specificity. *Brain* **114**, 775-788.
Lowe, J., Blanchard, A., Morrell, K., Lennox, G., Reynolds, L., Billett, M., Landon, M. and Mayer, R. J. (1988). Ubiquitin is a common factor in intermediate filament inclusion bodies of diverse type in man, including those of Parkinson's disease, Pick's disease, and Alzheimer's disease, as well as Rosenthal fibres in cerebellar astrocytomas, cytoplasmic bodies in muscle, and mallory bodies in alcoholic liver disease. *J. Pathol.* **155**, 9-15.
Mabb, A. M. and Ehlers, M. D. (2010). Ubiquitination in postsynaptic function and plasticity. *Annu. Rev. Cell Dev. Biol.* **26**, 179-210.
Maharjan, S., Oku, M., Tsuda, M., Hoseki, J. and Sakai, Y. (2014). Mitochondrial impairment triggers cytosolic oxidative stress and cell death following proteasome inhibition. *Sci. Rep.* **4**, 5896.
Mattiazzi, M., D'Aurelio, M., Gajewski, C. D., Martushova, K., Kiaei, M., Beal, M. F. and Manfredi, G. (2002). Mutated human SOD1 causes dysfunction of oxidative phosphorylation in mitochondria of transgenic mice. *J. Biol. Chem.* **277**, 29626-29633.
McAlary, L., Yerbury, J. J. and Aquilina, J. A. (2013). Glutathionylation potentiates benign superoxide dismutase 1 variants to the toxic forms associated with amyotrophic lateral sclerosis. *Sci. Rep.* **3**, 3275.
McAlary, L., Aquilina, J. A. and Yerbury, J. J. (2016). Susceptibility of mutant SOD1 to form a destabilized monomer predicts cellular aggregation and toxicity but not in vitro aggregation propensity. *Front. Neurosci.* **10**, 499.
Mimnaugh, E. G., Chen, H. Y., Davie, J. R., Celis, J. E. and Neckers, L. (1997). Rapid deubiquitination of nucleosomal histones in human tumor cells caused by proteasome inhibitors and stress response inducers: effects on replication, transcription, translation, and the cellular stress response. *Biochemistry* **36**, 14418-14429.
Miyazaki, K., Fujita, T., Ozaki, T., Kato, C., Kurose, Y., Sakamoto, M., Kato, S., Goto, T., Itoyama, Y., Aoki, M. et al. (2004). NEDL1, a novel ubiquitin-protein isopeptide ligase for dishevelled-1, targets mutant superoxide dismutase-1. *J. Biol. Chem.* **279**, 11327-11335.
Mori, H., Kondo, J. and Ihara, Y. (1987). Ubiquitin is a component of paired helical filaments in Alzheimer's disease. *Science* **235**, 1641-1644.
Münch, C., O'Brien, J. and Bertolotti, A. (2011). Prion-like propagation of mutant superoxide dismutase-1 misfolding in neuronal cells. *Proc. Natl. Acad. Sci. USA* **108**, 3548-3553.
Nagarajan, S. R., Brandon, A. E., McKenna, J. A., Shtein, H. C., Nguyen, T. Q., Suryana, E., Poronnik, P., Cooney, G. J., Saunders, D. N. and Hoy, A. J. (2017). Insulin and diet-induced changes in the ubiquitin-modified proteome of rat liver. *PLoS ONE* **12**, e0174431.
Patnaik, A., Chau, V. and Wills, J. W. (2000). Ubiquitin is part of the retrovirus budding machinery. *Proc. Natl. Acad. Sci. USA* **97**, 13069-13074.
Pickart, C. M. (2001). Mechanisms underlying ubiquitination. *Annu. Rev. Biochem.* **70**, 503-533.
Powis, R. A., Karyka, E., Boyd, P., Come, J., Jones, R. A., Zheng, Y., Szunyogova, E., Groen, E. J., Hunter, G., Thomson, D. et al. (2016). Systemic restoration of UBA1 ameliorates disease in spinal muscular atrophy. *JCI Insight* **1**, e87908.
Ruan, L., Zhou, C., Jin, E., Kucharavy, A., Zhang, Y., Wen, Z., Florens, L. and Li, R. (2017). Cytosolic proteostasis through importing of misfolded proteins into mitochondria. *Nature* **543**, 443-446.
Schneider, C. A., Rasband, W. S. and Eliceiri, K. W. (2012). NIH Image to ImageJ: 25 years of image analysis. *Nat. Methods* **9**, 671-675.
Scotter, E. L., Vance, C., Nishimura, A. L., Lee, Y. B., Chen, H. J., Urwin, H., Sardone, V., Mitchell, J. C., Rogelj, B., Rubinsztein, D. C. et al. (2014). Differential roles of the ubiquitin proteasome system and autophagy in the clearance of soluble and aggregated TDP-43 species. *J. Cell Sci.* **127**(Pt 6), 1263-1278.
Sherman, M. Y. and Goldberg, A. L. (2001). Cellular defenses against unfolded proteins: a cell biologist thinks about neurodegenerative diseases. *Neuron* **29**, 15-32.
Smoot, M. E., Ono, K., Ruscheinski, J., Wang, P. L. and Ideker, T. (2011). Cytoscape 2.8: new features for data integration and network visualization. *Bioinformatics* **27**, 431-432.
Song, W., Song, Y., Kincaid, B., Bossy, B. and Bossy-Wetzel, E. (2013). Mutant SOD1G93A triggers mitochondrial fragmentation in spinal cord motor neurons: neuroprotection by SIRT3 and PGC-1alpha. *Neurobiol. Dis.* **51**, 72-81.
Strong, M. J., Kesavapany, S. and Pant, H. C. (2005). The pathobiology of amyotrophic lateral sclerosis: A proteinopathy? *J. Neuropathol. Exp. Neurol.* **64**, 649-664.
Sundaramoorthy, V., Walker, A. K., Yerbury, J., Soo, K. Y., Farg, M. A., Hoang, V., Zeineddine, R., Spencer, D. and Atkin, J. D. (2013). Extracellular wildtype and mutant SOD1 induces ER-Golgi pathology characteristic of amyotrophic lateral sclerosis in neuronal cells. *Cell. Mol. Life Sci.* **70**, 4181-4195.
Szklarczyk, D., Franceschini, A., Wyder, S., Forslund, K., Heller, D., Huerta-Cepas, J., Simonovic, M., Roth, A., Santos, A., Tsafou, K. P. et al. (2015). STRING v10: protein-protein interaction networks, integrated over the tree of life. *Nucleic Acids Res.* **43**, D447-D452.
Tan, Z., Qu, W., Tu, W., Liu, W., Baudry, M. and Schreiber, S. S. (2000). p53 accumulation due to down-regulation of ubiquitin: relevance for neuronal apoptosis. *Cell Death Differ.* **7**, 675-681.
Tan, Z., Tu, W. and Schreiber, S. S. (2001). Downregulation of free ubiquitin: a novel mechanism of p53 stabilization and neuronal cell death. *Brain Res. Mol. Brain Res.* **91**, 179-188.
Tan, J. M., Wong, E. S., Kirkpatrick, D. S., Pletnikova, O., Ko, H. S., Tay, S. P., Ho, M. W., Troncoso, J., Gygi, S. P., Lee, M. K. et al. (2008). Lysine 63-linked ubiquitination promotes the formation and autophagic clearance of protein inclusions associated with neurodegenerative diseases. *Hum. Mol. Genet.* **17**, 431-439.
Tashiro, Y., Urushitani, M., Inoue, H., Koike, M., Uchiyama, Y., Komatsu, M., Tanaka, K., Yamazaki, M., Abe, M., Misawa, H. et al. (2012). Motor neuron-specific disruption of proteasomes, but not autophagy, replicates amyotrophic lateral sclerosis. *J. Biol. Chem.* **287**, 42984-42994.
Ticozzi, N., Ratti, A. and Silani, V. (2010). Protein aggregation and defective RNA metabolism as mechanisms for motor neuron damage. *CNS Neurol. Disord. Drug Targets* **9**, 285-296.
Tsvetkov, A. S., Arrasate, M., Barmada, S., Ando, D. M., Sharma, P., Shaby, B. A. and Finkbeiner, S. (2013). Proteostasis of polyglutamine varies among neurons and predicts neurodegeneration. *Nat. Chem. Biol.* **9**, 586-592.
Turner, B. J., Atkin, J. D., Farg, M. A., Zang, D. W., Rembach, A., Lopes, E. C., Patch, J. D., Hill, A. F. and Cheema, S. S. (2005). Impaired extracellular secretion of mutant superoxide dismutase 1 associates with neurotoxicity in familial amyotrophic lateral sclerosis. *J. Neurosci.* **25**, 108-117.
Turner, M. R., Hardiman, O., Benatar, M., Brooks, B. R., Chio, A., de Carvalho, M., Ince, P. G., Lin, C., Miller, R. G., Mitsumoto, H. et al. (2013). Controversies and priorities in amyotrophic lateral sclerosis. *Lancet Neurol.* **12**, 310-322.
Turriziani, B., Garcia-Munoz, A., Pilkington, R., Raso, C., Kolch, W. and von Kriegsheim, A. (2014). On-beads digestion in conjunction with data-dependent mass spectrometry: a shortcut to quantitative and dynamic interaction proteomics. *Biology*, 320-332.
Ugun-Klusek, A., Tatham, M. H., Elkharaz, J., Constantin-Teodosiu, D., Lawler, K., Mohamed, H., Paine, S. M., Anderson, G., John Mayer, R., Lowe, J. et al. (2017). Continued 26S proteasome dysfunction in mouse brain cortical neurons impairs autophagy and the Keap1-Nrf2 oxidative defence pathway. *Cell Death Dis.* **8**, e2531.
Vaden, J. H., Watson, J. A., Howard, A. D., Chen, P. C., Wilson, J. A. and Wilson, S. M. (2015). Distinct effects of ubiquitin overexpression on NMJ structure and motor performance in mice expressing catalytically inactive USP14. *Front. Mol. Neurosci.* **8**, 11.
Vande Velde, C., McDonald, K. K., Boukhedimi, Y., McAlonis-Downes, M., Lobsiger, C. S., Bel Hadj, S., Zandona, A., Julien, J. P., Shah, S. B. and Cleveland, D. W. (2011). Misfolded SOD1 associated with motor neuron mitochondria alters mitochondrial shape and distribution prior to clinical onset. *PLoS ONE* **6**, e22031.
Vijayvergiya, C., Beal, M. F., Buck, J. and Manfredi, G. (2005). Mutant superoxide dismutase 1 forms aggregates in the brain mitochondrial matrix of amyotrophic lateral sclerosis mice. *J. Neurosci.* **25**, 2463-2470.
Wang, H., Ying, Z. and Wang, G. (2012). Ataxin-3 regulates aggresome formation of copper-zinc superoxide dismutase (SOD1) by editing K63-linked polyubiquitin chains. *J. Biol. Chem.* **287**, 28576-28585.
Weisberg, S. J., Lyakhovetsky, R., Werdiger, A. C., Gitler, A. D., Soen, Y. and Kaganovich, D. (2012). Compartmentalization of superoxide dismutase 1 (SOD1G93A) aggregates determines their toxicity. *Proc. Natl. Acad. Sci. USA* **109**, 15811-15816.
Williams, K. L., Topp, S., Yang, S., Smith, B., Fifita, J. A., Warraich, S. T., Zhang, K. Y., Farrawell, N., Vance, C., Hu, X. et al. (2016). CCNF mutations in amyotrophic lateral sclerosis and frontotemporal dementia. *Nat. Commun.* **7**, 11253.
Wishart, T. M., Mutsaers, C. A., Riessland, M., Reimer, M. M., Hunter, G., Hannam, M. L., Eaton, S. L., Fuller, H. R., Roche, S. L., Somers, E. et al. (2014). Dysregulation of ubiquitin homeostasis and beta-catenin signaling promote spinal muscular atrophy. *J. Clin. Invest.* **124**, 1821-1834.
Yang, S., Zhang, K. Y., Kariawasam, R., Bax, M., Fifita, J. A., Ooi, L., Yerbury, J. J., Nicholson, G. A. and Blair, I. P. (2015). Evaluation of skin fibroblasts from amyotrophic lateral sclerosis patients for the rapid study of pathological features. *Neurotox. Res.* **28**, 138-146.
Yerbury, J. J. and Kumita, J. R. (2010). Protein chemistry of amyloid fibrils and chaperones: Implications for amyloid formation and disease. *Curr. Chem. Biol.* **4**, 89-98.

Yerbury, J. J., Ooi, L., Dillin, A., Saunders, D. N., Hatters, D. M., Beart, P. M., Cashman, N. R., Wilson, M. R. and Ecroyd, H. (2016). Walking the tightrope: proteostasis and neurodegenerative disease. *J. Neurochem.* **137**, 489-505.

Yonashiro, R., Sugiura, A., Miyachi, M., Fukuda, T., Matsushita, N., Inatome, R., Ogata, Y., Suzuki, T., Dohmae, N. and Yanagi, S. (2009). Mitochondrial ubiquitin ligase MITOL ubiquitinates mutant SOD1 and attenuates mutant SOD1-induced reactive oxygen species generation. *Mol. Biol. Cell* **20**, 4524-4530.

Zeineddine, R., Pundavela, J. F., Corcoran, L., Stewart, E. M., Do-Ha, D., Bax, M., Guillemin, G., Vine, K. L., Hatters, D. M., Ecroyd, H. et al. (2015). SOD1 protein aggregates stimulate macropinocytosis in neurons to facilitate their propagation. *Mol. Neurodegener.* **10**, 57.